

# A GLOBALLY DIVERGENCE-FREE ENTROPY STABLE NODAL DG METHOD FOR CONSERVATIVE IDEAL MHD EQUATIONS\*

YUCHANG LIU<sup>†</sup>, WEI GUO<sup>‡</sup>, YAN JIANG<sup>§</sup>, AND MENGPIG ZHANG<sup>¶</sup>

**Abstract.** We propose an arbitrarily high-order globally divergence-free entropy stable nodal discontinuous Galerkin (DG) method to directly solve the conservative form of the ideal MHD equations using appropriate quadrature rules. The method ensures a globally divergence-free magnetic field by updating it at interfaces with a constraint-preserving formulation [5] and employing a novel least-squares reconstruction technique. Leveraging this property, the semi-discrete nodal DG scheme is proven to be entropy stable. To handle the problems with strong shocks, we introduce a novel limiting strategy that suppresses unphysical oscillations while preserving the globally divergence-free property. Numerical experiments verify the accuracy and efficacy of our method.

**Key words.** discontinuous Galerkin method, ideal MHD equation, globally divergence-free, entropy stability, high-order accuracy.

**MSC codes.** 65M60, 76W05.

**1. Introduction.** In this paper, we focus on simulating the compressible ideal magnetohydrodynamic (MHD) equations, which describe the dynamics of perfectly conducting fluids and have a wide range of applications in space weather forecasting, astrophysics, plasma physics, among others. The ideal MHD equations are derived by combining the Euler equations from fluid dynamics and pre-Maxwell's equations from electromagnetism and are formulated as a set of nonlinear hyperbolic conservation laws, along with a divergence-free constraint on the magnetic field. Solving the MHD equations accurately and reliably presents significant challenges. As with other nonlinear conservation laws, the desired entropy solution of the MHD equations is known to develop discontinuities and other complex solution features in finite time and satisfy the entropy inequality, aligning with the second law of thermodynamics. In addition, if the magnetic field is initially divergence-free, it will remain so for all time, reflecting the absence of magnetic monopoles in nature. Failure to preserve these physical constraints on the discrete level may lead to unphysical artifacts and instability of MHD simulations [4]. In this work, we aim for a globally divergence-free shock capture MHD solver that further fulfills a discrete entropy inequality, termed entropy stability.

In recent years, various effective high-order methods have been proposed to solve the MHD equations, including finite difference methods [1, 17, 47], finite volume methods [27], spectral methods [52, 44], finite element methods [36], and discontinuous Galerkin (DG) methods [39, 42, 5]. In this work, we utilize the DG discretization [50, 21, 20, 18, 22, 23], leveraging its well-known advantages, such as high order accuracy, good conservation properties, the ability to handle hanging nodes, and high parallel efficiency. Furthermore, its flexibility enables the design of effective techniques

---

\*Submitted to the editors DATE.

<sup>†</sup>School of Mathematical Sciences, University of Science and Technology of China, Hefei, Anhui 230026, P.R. China. (lissandra@mail.ustc.edu.cn).

<sup>‡</sup>Department of Mathematics and Statistics, Texas Tech University, Lubbock, TX, 79409, USA. (weimath.guo@ttu.edu). Research supported by NSF grant NSF-DMS-2111383, Air Force Office of Scientific Research FA9550-18-1-0257.

<sup>§</sup> School of Mathematical Sciences, University of Science and Technology of China, Hefei, Anhui 230026, P.R. China. (jiangy@ustc.edu.cn). Research supported by NSFC grant 12271499.

<sup>¶</sup> School of Mathematical Sciences, University of Science and Technology of China, Hefei, Anhui 230026, P.R. China. (mpzhang@ustc.edu.cn).

to enforce the desired constraints, specifically the divergence-free property and entropy stability.

To achieve the divergence-free property, several effective approaches have been proposed in the literature, including the 8-wave formulation [49], the projection methods [56], hyperbolic divergence-cleaning technique [25], and the constrained transport (CT) method [26, 3, 17, 59]. In the context of DG discretization, a locally divergence-free DG method was developed in [39], which employs a piecewise divergence-free polynomial vector space to approximate the magnetic field. In [40], the globally divergence-free central DG methods involving two copies of solutions were formulated for solving the two-dimensional ideal MHD equation. In such methods, the magnetic field is approximated within the exactly divergence-free  $H(\text{div})$ -conforming Brezzi–Douglas–Marini finite element space [9]. In particular, this method defines the magnetic field components on the interface as univariate polynomials, utilizing them at each time step to reconstruct the magnetic field, thereby ensuring the magnetic field is divergence-free internally and continuous in the normal direction. In [29], Fu *et al.* extended it to DG method by using multidimensional Riemann solver at vertices. The magnetic field reconstruction requirements of the above two methods do not explicitly contain the divergence-free constraint, and the divergence-free property is guaranteed by a theorem, in which the scheme on the boundary and internal must be closely related. However, for shock problems, they fail in designing a limiter for the magnetic field at interfaces since the limiter will destroy the theorem. Balsara *et al.* made an improvement in [5]. Their reconstruction requirements explicitly contain the divergence-free constraint, hence the reconstruction is compatible with the limiter.

Meanwhile, the development of entropy stable numerical methods for hyperbolic conservation laws has attracted significant research interest over the past two decades, as they are crucial for capturing the physically relevant solution that obeys the second law of thermodynamics. For instance, the famous high order entropy stable finite volume ENO scheme, termed the TeCNO scheme, was developed in [28], leveraging fundamental techniques such as entropy conservative and entropy stable fluxes [54, 55] and the sign property of ENO reconstruction [24]. For DG discretization, two primary approaches have been developed to ensure entropy stability. The first approach utilizes the summation-by-parts (SBP) methodology [32]. In [15], Chen and Shu constructed the entropy stable nodal DG method by introducing SBP operators on Gauss-Lobatto points in conjunction. In [11, 12], it was extended to modal DG formulation by designing the hybridized SBP operators that combine the volume and surface quadrature nodes. The second approach aims to explicitly control the production of entropy within each element by adding an artificial term, see [2, 30, 41].

In [35], Godunov pointed out that the ideal MHD equations with the divergence-free constraint are not symmetrizable, unless an additional source term is included, which vanishes if the magnetic field is divergence-free. A symmetrizable hyperbolic system is guaranteed to possess an entropy function. Hence, entropy analysis and the divergence-free condition are closely related at both the PDE and discrete levels. In [13], Chandrashekar *et al.* proposed an entropy stable finite volume entropy scheme for this modified symmetrizable form of MHD by introducing a novel entropy conservative flux. In [42], Liu *et al.* extended this approach to construct an entropy stable nodal DG method by carefully handling the added source term. However, since both methods do not satisfy the divergence-free constraint at the discrete level, they are inherently nonconservative by discretizing the modified MHD equations. This can lead to numerical instability and nonphysical features in the approximated solutions [56, 13]. In this work, we follow the entropy stable nodal DG framework [42] and inte-

grate the globally divergence-free technique [5]. This allows us to directly simulate the conservative form of the ideal MHD equations, as opposed to the existing approaches, ensuring both entropy stability and globally divergence-free conditions. For problems with strong shocks, we develop a scaling limiter to suppress unphysical oscillations, inspired by the key idea of the oscillation-free DG method and subsequent works [43, 48, 57]. This limiter preserves both entropy stability and the divergence-free property.

The contributions of this work are summarized as follows:

1. The magnetic field is globally divergence-free.
2. The semi-discrete scheme in each cell is entropy stable.
3. The framework conserves locally the mass, momentum and magnetic field, while total energy conservation is not maintained. Such a conservation error depends on the on the discrepancy between the magnetic field before and after the reconstruction step.

The rest of this paper is organized as follows: Section 2 introduces the ideal MHD equations and the associated entropy condition. Section 3 presents the proposed globally divergence-free entropy stable (ES-GDF) nodal DG scheme for the conservative form of MHD, along with a theoretical analysis. Section 4 describes a consistent limiting strategy that preserves both entropy stability and the globally divergence-free property, as well as the fully discrete formulation. In Section 5, various numerical examples are provided to demonstrate the efficiency and effectiveness of the proposed scheme. Section 6 concludes with a discussion of the findings.

## 2. Ideal MHD equations.

**2.1. Governing equations.** In this paper, we consider the two-dimensional ideal MHD equations in Cartesian coordinates, formulated as a system of conservation laws

$$(2.1) \quad \frac{\partial \mathbf{U}}{\partial t} + \frac{\partial \mathbf{F}(\mathbf{U})}{\partial x} + \frac{\partial \mathbf{G}(\mathbf{U})}{\partial y} = \mathbf{0},$$

where  $\mathbf{U} = (\rho, u_x, u_y, u_z, \mathcal{E}, B_x, B_y, B_z)^T$ , and

$$\mathbf{F}(\mathbf{U}) = \begin{bmatrix} \rho u_x \\ \rho u_x^2 + p^* - B_x^2 \\ \rho u_x u_y - B_x B_y \\ \rho u_x u_z - B_x B_z \\ u_x (\mathcal{E} + p^*) - B_x (\mathbf{u} \cdot \mathbf{B}) \\ 0 \\ u_x B_y - u_y B_x \\ u_x B_z - u_z B_x \end{bmatrix}, \quad \mathbf{G}(\mathbf{U}) = \begin{bmatrix} \rho u_y \\ \rho u_x u_y - B_x B_y \\ \rho u_y^2 + p^* - B_y^2 \\ \rho u_y u_z - B_y B_z \\ u_y (\mathcal{E} + p^*) - B_y (\mathbf{u} \cdot \mathbf{B}) \\ u_y B_x - u_x B_y \\ 0 \\ u_y B_z - u_z B_y \end{bmatrix},$$

with

$$(2.2) \quad \mathcal{E} = \frac{p}{\gamma - 1} + \frac{1}{2} \rho \|\mathbf{u}\|^2 + \frac{1}{2} \|\mathbf{B}\|^2.$$

Here,  $\rho$  represents the mass density,  $\rho \mathbf{u}$  is the momentum,  $\mathcal{E}$  denotes the total energy,  $p$  is the hydrodynamic pressure,  $\mathbf{B}$  represents the magnetic field,  $\gamma = 5/3$  is the ideal gas constant,  $p^* = p + \|\mathbf{B}\|^2/2$  is the total pressure, and  $\|\cdot\|$  denotes the Euclidean vector norm. Taking divergence of the magnetic field equation yields  $\frac{\partial(\nabla \cdot \mathbf{B})}{\partial t} = 0$ ,

indicating  $\nabla \cdot \mathbf{B}(\mathbf{x}, t) = \nabla \cdot \mathbf{B}(\mathbf{x}, 0)$ . Consequently, if the divergence of the magnetic field is initially zero, it will remain zero for all time, i.e.

$$(2.3) \quad \nabla \cdot \mathbf{B} = 0.$$

This is called the *divergence-free property*. Preservation of the discrete divergence-free property in MHD simulations is critical to prevent unphysical artifacts and numerical instabilities.

**2.2. Entropy analysis for the ideal MHD equations.** It is well-known that weak solutions to conservation laws are not unique. Imposing an entropy condition ensures uniqueness for scalar problems [33], although for systems, the uniqueness remains an open problem. Nevertheless, the entropy condition is a valuable design principle that enhances numerical stability and ensures compliance with the second law of thermodynamics.

**DEFINITION 2.1.** *A convex scalar function  $\mathcal{U}(\mathbf{U})$  is called an entropy function of system (2.1), if there exist scalar entropy fluxes  $\mathcal{F}(\mathbf{U})$  and  $\mathcal{G}(\mathbf{U})$  such that*

$$(2.4) \quad \mathcal{F}'(\mathbf{U}) = \mathcal{U}'(\mathbf{U}) \mathbf{F}'(\mathbf{U}), \quad \mathcal{G}'(\mathbf{U}) = \mathcal{U}'(\mathbf{U}) \mathbf{G}'(\mathbf{U}).$$

*The functions  $(\mathcal{U}, \mathcal{F}, \mathcal{G})$  are called an entropy pair. Here,  $\mathcal{U}'(\mathbf{U})$ ,  $\mathcal{F}'(\mathbf{U})$ ,  $\mathcal{G}'(\mathbf{U})$  are viewed as row vectors, and  $\mathbf{F}'(\mathbf{U})$ ,  $\mathbf{G}'(\mathbf{U})$  are the Jacobian matrixes.*

If a system of conservation law admits an entropy pair, a weak solution that further satisfies the following inequality in the weak sense is called the *entropy solution*,

$$(2.5) \quad \frac{\partial \mathcal{U}(\mathbf{U})}{\partial t} + \frac{\partial \mathcal{F}(\mathbf{U})}{\partial x} + \frac{\partial \mathcal{G}(\mathbf{U})}{\partial y} \leq 0,$$

which is known as the *entropy condition*. In particular, this inequality becomes an equality for smooth solutions.

Define the entropy variable  $\mathbf{V} = \mathcal{U}'(\mathbf{U})^T$ . If  $\mathcal{U}$  is strictly convex, the mapping  $\mathbf{U} \rightarrow \mathbf{V}$  is one-to-one. It is known that the existence of an entropy pair is closely related to the symmetrization of the underlying system of conservation laws. In particular, the system (2.1) possesses a strictly convex entropy function  $\mathcal{U}$  if and only if  $\partial \mathbf{U} / \partial \mathbf{V}$  is a symmetric, positive definite matrix and  $\partial \mathbf{F}(\mathbf{U}(\mathbf{V})) / \partial \mathbf{V}$ ,  $\partial \mathbf{G}(\mathbf{U}(\mathbf{V})) / \partial \mathbf{V}$  are symmetric matrices [34]. Therefore, if the transformation  $\mathbf{U} \rightarrow \mathbf{V}$  symmetrizes the system, then there exist twice differentiable scalar functions  $\varphi(\mathbf{V})$ ,  $\psi_F(\mathbf{V})$ ,  $\psi_G(\mathbf{V})$  with  $\varphi(\mathbf{V})$  being strictly convex such that

$$\mathbf{U}(\mathbf{V})^T = \frac{\partial \varphi}{\partial \mathbf{V}}, \quad \mathbf{F}(\mathbf{V})^T = \frac{\partial \psi_F}{\partial \mathbf{V}}, \quad \mathbf{G}(\mathbf{V})^T = \frac{\partial \psi_G}{\partial \mathbf{V}},$$

where  $\frac{\partial \varphi}{\partial \mathbf{V}}$ ,  $\frac{\partial \psi_F}{\partial \mathbf{V}}$ ,  $\frac{\partial \psi_G}{\partial \mathbf{V}}$  are viewed as row vectors. It is straightforward to verify that

$$\begin{aligned} \varphi(\mathbf{V}) &= \mathbf{V}^T \mathbf{U}(\mathbf{V}) - \mathcal{U}(\mathbf{U}(\mathbf{V})), \\ \psi_F(\mathbf{V}) &= \mathbf{V}^T \mathbf{F}(\mathbf{U}(\mathbf{V})) - \mathcal{F}(\mathbf{U}(\mathbf{V})), \\ \psi_G(\mathbf{V}) &= \mathbf{V}^T \mathbf{G}(\mathbf{U}(\mathbf{V})) - \mathcal{G}(\mathbf{U}(\mathbf{V})). \end{aligned}$$

The entropy pair for ideal MHD equations is introduced in light of the thermodynamic entropy  $s = \ln(p\rho^{-\gamma})$ . In particular, the following equation for  $\rho s$  can be derived from the MHD equation:

$$\frac{\partial \rho s}{\partial t} + \frac{\partial \rho u_x s}{\partial x} + \frac{\partial \rho u_y s}{\partial y} + (\gamma - 1) \frac{\rho(\mathbf{u} \cdot \mathbf{B})}{p} (\nabla \cdot \mathbf{B}) = 0.$$

We can verify that the following pair satisfies the condition (2.5)

$$(2.6) \quad \mathcal{U} = -\frac{\rho s}{\gamma - 1}, \quad \mathcal{F} = -\frac{\rho u_x s}{\gamma - 1}, \quad \mathcal{G} = -\frac{\rho u_y s}{\gamma - 1},$$

and consequently,  $\mathbf{V}$  is given by

$$\mathbf{V} = \left( \frac{\partial \mathcal{U}}{\partial \mathbf{U}} \right)^T = \left[ \frac{\gamma - s}{\gamma - 1} - \beta \|\mathbf{u}\|^2, 2\beta \mathbf{u}, -2\beta, 2\beta \mathbf{B} \right]^T, \quad \beta = \frac{\rho}{2p}.$$

However, the change of variables  $\mathbf{U} \rightarrow \mathbf{V}$  fails to symmetrize the ideal MHD equations (2.1), and hence  $(\mathcal{U}, \mathcal{F}, \mathcal{G})$  does not constitute an entropy pair. To overcome the difficulty, Godunov [35] introduced a modified form

$$(2.7) \quad \frac{\partial \mathbf{U}}{\partial t} + \frac{\partial \mathbf{F}(\mathbf{U})}{\partial x} + \frac{\partial \mathbf{G}(\mathbf{U})}{\partial y} + \phi'(\mathbf{V})^T \nabla \cdot \mathbf{B} = 0$$

with  $\phi(\mathbf{V}) = 2\beta(\mathbf{u} \cdot \mathbf{B})$ , which can be symmetrized with the above transformation  $\mathbf{U} \rightarrow \mathbf{V}$ . Since  $\nabla \cdot \mathbf{B} = 0$ , the above modification is consistent with the ideal MHD equation (2.1). In particular,  $\phi(\mathbf{V})$  is a homogeneous function of degree one, that is  $\mathbf{V} \cdot \phi'(\mathbf{V})^T = \phi(\mathbf{V})$ , with Jacobian matrix  $\phi'(\mathbf{V}) = [0, \mathbf{B}, \mathbf{u} \cdot \mathbf{B}, \mathbf{u}]$ .

**3. Globally divergence-free entropy stable nodal DG scheme for the conservative form of MHD.** The modified MHD equation (2.7) is equivalent to the original conservative form (2.1) only if the magnetic field is divergence-free. Many existing entropy stable numerical schemes discretize the modified form (2.7), and the additional term is treated as a non-conservative source term. Thus, without strictly preserving the divergence-free property, such schemes can ensure the mass conservation but may fail to conserve other quantities, including the momentum, total energy, and magnetic field. Meanwhile, only conservative schemes can guarantee the correct jump conditions and capture a weak solution upon convergence [56]. Hence, non-conservative schemes are susceptible to producing non-physical results, as demonstrated in the literature [56, 13, 42, 58]. To partly address the difficulty, we propose to develop a globally divergence-free scheme, enabling us to discrete the conservative form (2.1) while still ensuring the entropy condition.

**3.1. Nodal DG method for conservation laws.** The proposed method follows the methodology in [15], which established a general framework for designing entropy stable nodal DG schemes for hyperbolic conservation laws. The main ingredients include SBP operators derived from the Gauss-Lobatto quadrature, the entropy conservative flux within elements, and the entropy stable flux at element interfaces. This approach has been successfully applied to the ideal MHD in the non-conservative form [42].

Assume that the 2D spatial domain  $\Omega = [a, b] \times [c, d]$  is divided into a  $N_x \times N_y$  uniform rectangular mesh with cells  $\mathcal{K} = \{K_{ij} = [x_{i-1/2}, x_{i+1/2}] \times [y_{j-1/2}, y_{j+1/2}]\}$ , and the step sizes in  $x$  and  $y$  directions are denoted by  $\Delta x$  and  $\Delta y$ , respectively.

Denote the  $k + 2$  Gauss-Lobatto quadrature points

$$-1 = X_0 < X_1 < \cdots < X_{k+1} = 1,$$

and the associated quadrature weights  $\{\omega_l\}_{l=0}^{k+1}$  over the reference element  $I = [-1, 1]$ . The difference matrix  $D$  is defined as  $D_{jl} = L_l'(X_j)$ , where  $L_l$  is the  $l$ -th Lagrange basis polynomial satisfying  $L_l(X_j) = \delta_{lj}$ , and the mass matrix  $M$  and the stiffness matrix  $S$  are defined as  $M = \text{diag}\{\omega_0, \omega_1, \dots, \omega_{k+1}\}$ ,  $S = MD$ . We recall the properties of these matrices [15]:

LEMMA 3.1. *Set the boundary matrix*

$$B = \text{diag}\{-1, 0, 0, \dots, 0, 0, 1\} =: \text{diag}\{\tau_0, \dots, \tau_{k+1}\},$$

then  $S + S^T = B$ .

LEMMA 3.2. *For each  $0 \leq j \leq k+1$ ,*

$$\sum_{l=0}^{k+1} D_{jl} = \sum_{l=0}^{k+1} S_{jl} = 0, \quad \sum_{l=0}^{k+1} S_{lj} = \tau_j.$$

We further introduce some useful notations. Define the piecewise tensor-product polynomial space

$$V_h = \{w(x, y) : w(x, y)|_{K_{ij}} \in Q^{k+1}(K_{ij}), \forall K_{ij} \in \mathcal{K}\},$$

where  $Q^{k+1}(K_{ij})$  denotes the set of tensor-product polynomials of degree at most  $k+1$  over cell  $K_{ij}$ . Denote the DG solution  $\mathbf{U}_h \in [V_h]^8$  that approximates  $\mathbf{U}$ . Let

$$x_i(X) = x_i + \frac{\Delta x}{2}X, \quad y_j(Y) = y_j + \frac{\Delta y}{2}Y,$$

and denote the nodal values at the local quadrature points by

$$\mathbf{U}_{i_1, j_1}^{i, j} = \mathbf{U}_h(x_i(X_{i_1}), y_j(Y_{j_1})).$$

Then the solution is represented by

$$\mathbf{U}_h|_{K_{ij}} = \sum_{i_1, j_1=0}^{k+1} \mathbf{U}_{i_1, j_1}^{i, j} L_{i_1} \left( \frac{x - x_i}{\Delta x/2} \right) L_{j_1} \left( \frac{y - y_j}{\Delta y/2} \right).$$

Denote the nodal values  $\mathbf{F}_{i_1, j_1}^{i, j} = \mathbf{F}(\mathbf{U}_{i_1, j_1}^{i, j})$  and  $\mathbf{G}_{i_1, j_1}^{i, j} = \mathbf{G}(\mathbf{U}_{i_1, j_1}^{i, j})$ , and define

$$\mathbf{F}_{i_1, j_1}^{*, i, j} = \begin{cases} \hat{\mathbf{F}}(\mathbf{U}_{k+1, j_1}^{i-1, j}, \mathbf{U}_{0, j_1}^{i, j}) =: \hat{\mathbf{F}}_{j_1}^{i-1/2, j}, & i_1 = 0, \\ \mathbf{0}, & 1 \leq i_1 \leq k, \\ \hat{\mathbf{F}}(\mathbf{U}_{k+1, j_1}^{i, j}, \mathbf{U}_{0, j_1}^{i+1, j}) =: \hat{\mathbf{F}}_{j_1}^{i+1/2, j}, & i_1 = k+1, \end{cases}$$

$$\mathbf{G}_{i_1, j_1}^{*, i, j} = \begin{cases} \hat{\mathbf{G}}(\mathbf{U}_{i_1, k+1}^{i, j-1}, \mathbf{U}_{i_1, 0}^{i, j}) =: \hat{\mathbf{G}}_{i_1}^{i, j-1/2}, & j_1 = 0, \\ \mathbf{0}, & 1 \leq j_1 \leq k, \\ \hat{\mathbf{G}}(\mathbf{U}_{i_1, k+1}^{i, j}, \mathbf{U}_{i_1, 0}^{i, j+1}) =: \hat{\mathbf{G}}_{i_1}^{i, j+1/2}, & j_1 = k+1. \end{cases}$$

Here,  $\hat{\mathbf{F}}(\cdot, \cdot)$ ,  $\hat{\mathbf{G}}(\cdot, \cdot)$  are the numerical fluxes at interfaces.

Following [15], the proposed nodal DG scheme for the ideal MHD equations in the conservative form (2.1) is given by

$$(3.1) \quad \begin{aligned} \frac{d\mathbf{U}_{i_1, j_1}^{i, j}}{dt} = & -\frac{2}{\Delta x} \sum_{l=0}^{k+1} 2D_{i_1, l} \mathbf{F}^S(\mathbf{U}_{i_1, j_1}^{i, j}, \mathbf{U}_{l, j_1}^{i, j}) + \frac{2}{\Delta x} \frac{\tau_{i_1}}{\omega_{i_1}} (\mathbf{F}_{i_1, j_1}^{i, j} - \mathbf{F}_{i_1, j_1}^{*, i, j}) \\ & -\frac{2}{\Delta y} \sum_{l=0}^{k+1} 2D_{j_1, l} \mathbf{G}^S(\mathbf{U}_{i_1, j_1}^{i, j}, \mathbf{U}_{i_1, l}^{i, j}) + \frac{2}{\Delta y} \frac{\tau_{j_1}}{\omega_{j_1}} (\mathbf{G}_{i_1, j_1}^{i, j} - \mathbf{G}_{i_1, j_1}^{*, i, j}), \end{aligned}$$

for  $1 \leq i \leq N_x$ ,  $1 \leq j \leq N_y$ ,  $0 \leq i_1, j_1 \leq k+1$ . Note that the scheme is represented as a matrix vector formulation based on nodal values. Here,  $\mathbf{F}^S(\mathbf{U}_L, \mathbf{U}_R)$  and  $\hat{\mathbf{F}}(\mathbf{U}_L, \mathbf{U}_R)$  are the entropy conservative flux and the entropy stable flux, respectively, which are defined as follows.

DEFINITION 3.3. A consistent, symmetric two-point numerical flux  $\mathbf{F}^S(\mathbf{U}_L, \mathbf{U}_R)$  is called entropy conservative, if for the given entropy function  $\mathcal{U}$ ,

$$(3.2) \quad (\mathbf{V}_R - \mathbf{V}_L)^T \mathbf{F}^S(\mathbf{U}_L, \mathbf{U}_R) = (\psi_R - \psi_L) - (\phi_R - \phi_L) \frac{B_{x,R} + B_{x,L}}{2}.$$

In particular,  $\mathbf{F}^S(\mathbf{U}, \mathbf{U}) = \mathbf{F}(\mathbf{U})$ .

DEFINITION 3.4. A consistent two-point numerical flux  $\hat{\mathbf{F}}(\mathbf{U}_L, \mathbf{U}_R)$  is called entropy stable, if for the given entropy function  $\mathcal{U}$ ,

$$(3.3) \quad (\mathbf{V}_R - \mathbf{V}_L)^T \hat{\mathbf{F}}(\mathbf{U}_L, \mathbf{U}_R) \leq (\psi_R - \psi_L) - (\phi_R - \phi_L) \frac{B_{x,R} + B_{x,L}}{2}.$$

In this paper, we employ the entropy conservative flux proposed by Chandrashekar and Klingenberg [13], along with the HLL numerical flux with suitable wave speed estimate [7, 8] as the entropy stable flux. For more details, see Appendix A.

It was proved in [15] that the nodal DG framework achieves the discrete entropy stability for a class of hyperbolic conservation laws, including the compressible Euler equation. Moreover, with the  $k+2$  Gauss-Lobatto quadrature points, the truncation error of the scheme is of  $(k+1)$ -th order at each collocation point. However, since the scheme (3.1) approximates the original conservative form of the MHD equations without preserving the divergence-free property, it cannot achieve the entropy stability. To address this, a globally divergence-free mechanism must be incorporated.

In the DG framework [5], the globally divergence-free property can be achieved through two conditions: the magnetic field must be locally divergence-free within each cell, and it must be continuous in the normal direction across cell interfaces. In particular, for the nodal DG formulation, the definition of a globally divergence-free magnetic field is given as follows.

DEFINITION 3.5. A magnetic field represented by nodal values on Gauss-Lobatto points  $\{\mathbf{B}_{i_1, j_1}^{i, j}\}_{i_1, j_1=0,0}^{k+1, k+1}$  is globally divergence-free, if

$$(3.4) \quad \sum_{l=0}^{k+1} \left( \frac{2}{\Delta x} D_{i_1, l} B_{x, l, j_1}^{i, j} + \frac{2}{\Delta y} D_{j_1, l} B_{y, i_1, l}^{i, j} \right) = 0,$$

$$(3.5) \quad B_{x, k+1, j_1}^{i, j} = B_{x, 0, j_1}^{i+1, j} =: B_{x, j_1}^{i+1/2, j}, \quad B_{y, i_1, k+1}^{i, j} = B_{y, i_1, 0}^{i, j+1} =: B_{y, i_1}^{i, j+1/2}$$

for any  $i, j, i_1, j_1$ .

Note that condition (3.4) indicates that the divergence of the magnetic field is zero at each quadrature point. Meanwhile, condition (3.5) implies that  $B_{x,h}$  and  $B_{y,h}$  are continuous along the  $x$ -direction and  $y$ -direction, respectively. With a globally divergence-free magnetic field satisfying (3.4)-(3.5), we are able to establish the following theorem for the proposed nodal DG scheme (3.1). The proof is given in Appendix C.

THEOREM 3.6. Assume that the boundary conditions are periodic, compactly supported, or reflective. If  $\mathbf{U}_h$  has a globally divergence-free magnetic field satisfying

(3.4) and (3.5), then the scheme (3.1) is entropy conservative within a single element

$$(3.6) \quad \begin{aligned} & \frac{d}{dt} \left( \frac{\Delta x \Delta y}{4} \sum_{i_1, j_1=0}^{k+1} \omega_{i_1} \omega_{j_1} \mathcal{U}_{i_1, j_1}^{i, j} \right) \\ &= - \sum_{j_1=0}^{k+1} \frac{\Delta y}{2} \omega_{j_1} \left( \mathcal{F}_{k+1, j_1}^{*, i, j} - \mathcal{F}_{0, j_1}^{*, i, j} \right) - \sum_{i_1=0}^{k+1} \frac{\Delta x}{2} \omega_{i_1} \left( \mathcal{G}_{i_1, k+1}^{*, i, j} - \mathcal{G}_{i_1, 0}^{*, i, j} \right), \end{aligned}$$

and entropy stable on the entire computational domain  $\Omega$  in the sense of

$$(3.7) \quad \frac{d}{dt} \int_{\Omega} \mathcal{U}(\mathbf{U}_h) dx dy \approx \frac{d}{dt} \left( \frac{\Delta x \Delta y}{4} \sum_{i, j=1}^{N_x, N_y} \sum_{i_1, j_1=0}^{k+1} \omega_{i_1} \omega_{j_1} \mathcal{U}_{i_1, j_1}^{i, j} \right) \leq 0,$$

where

$$\begin{aligned} \mathcal{F}_{k+1, j_1}^{*, i, j} &= \left( \mathbf{V}_{k+1, j_1}^{i, j} \right)^T \mathbf{F}_{k+1, j_1}^{*, i, j} - \psi_{F, k+1, j_1}^{i, j} + \phi_{k+1, j_1}^{i, j} B_{x, j_1}^{i+1/2, j}, \\ \mathcal{F}_{0, j_1}^{*, i, j} &= \left( \mathbf{V}_{0, j_1}^{i, j} \right)^T \mathbf{F}_{0, j_1}^{*, i, j} - \psi_{F, 0, j_1}^{i, j} + \phi_{0, j_1}^{i, j} B_{x, j_1}^{i-1/2, j}, \\ \mathcal{G}_{i_1, k+1}^{*, i, j} &= \left( \mathbf{V}_{i_1, k+1}^{i, j} \right)^T \mathbf{G}_{i_1, k+1}^{*, i, j} - \psi_{G, i_1, k+1}^{i, j} + \phi_{i_1, k+1}^{i, j} B_{y, i_1}^{i, j+1/2}, \\ \mathcal{G}_{i_1, 0}^{*, i, j} &= \left( \mathbf{V}_{i_1, 0}^{i, j} \right)^T \mathbf{G}_{i_1, 0}^{*, i, j} - \psi_{G, i_1, 0}^{i, j} + \phi_{i_1, 0}^{i, j} B_{y, i_1}^{i, j-1/2}. \end{aligned}$$

**3.2. Globally divergence-free method for B.** To achieve the globally divergence-free property under the DG framework, in [5] the authors proposed approximating the magnetic field components on the cell interface as univariate polynomials and utilizing them to reconstruct the magnetic field within each cell, ensuring it is divergence-free internally and continuous in the normal direction. The reconstructed magnetic field then replaces the one solved directly from the conservation laws (2.1). Moreover, to guarantee the existence of such a reconstruction, the degree of polynomials at the interfaces should be one degree lower than that of the polynomials within the cell. In particular, we seek the univariate polynomials of degree  $k$

$$b_x^{i+1/2, j}(y) \in P^k \left( I_{i+1/2, j}^y \right), \quad b_y^{i, j+1/2}(x) \in P^k \left( I_{i, j+1/2}^x \right),$$

which approximate  $B_x$  and  $B_y$  on cell interface  $I_{i+1/2, j}^y$  and  $I_{i, j+1/2}^x$ , respectively. Moreover, denote by  $E_z = u_y B_x - u_x B_y$ , then  $B_x$  and  $B_y$  satisfy

$$(3.8) \quad \frac{\partial B_x}{\partial t} + \frac{\partial E_z}{\partial y} = 0, \quad \frac{\partial B_y}{\partial t} - \frac{\partial E_z}{\partial x} = 0,$$

which can be treated as one-dimensional PDEs, and the following DG weak formulations are used to update  $b_x^{i+1/2, j}$  and  $b_y^{i, j+1/2}$  on interfaces:

$$(3.9) \quad \begin{aligned} \int_{I_{i+1/2, j}^y} \frac{\partial b_x^{i+1/2, j}}{\partial t} w dy &= \int_{I_{i+1/2, j}^y} \hat{E}_z^{i+1/2, j} \frac{\partial w}{\partial y} dy - \tilde{E}_z^{i+1/2, j+1/2} w(y_{j+1/2}^-) \\ &\quad + \tilde{E}_z^{i+1/2, j-1/2} w(y_{j-1/2}^+), \quad \forall w \in P^k \left( I_{i+1/2, j}^y \right), \end{aligned}$$



$$(3.10) \quad \int_{I_{i,j+1/2}^x} \frac{\partial \hat{b}_y^{i,j+1/2}}{\partial t} w dx = - \int_{I_{i,j+1/2}^x} \hat{E}_z^{i,j+1/2} \frac{\partial w}{\partial x} dx + \tilde{E}_z^{i+1/2,j+1/2} w(x_{i+1/2}^-) - \tilde{E}_z^{i-1/2,j+1/2} w(x_{i-1/2}^+), \quad \forall w \in P^k(I_{i,j+1/2}^x).$$

Note that  $\hat{E}_z^{i+1/2,j}$  is the 7th component of  $-\hat{\mathbf{F}}^{i+1/2,j}$ , and  $\hat{E}_z^{i,j+1/2}$  is the 6th component of  $\hat{\mathbf{G}}^{i,j+1/2}$ , respectively.  $w^\pm$  are the one-side limiting values of  $w$  at the interface.  $\tilde{E}_z^{i+1/2,j+1/2}$  is the two-dimensional Riemann solver defined at the vertex  $(x_{i+1/2}, y_{j+1/2})$ , which is single-valued and depends on the limiting states  $\mathbf{U}_{i+1/2,j+1/2}^{\pm,\pm}$  from four surrounding cells

$$\tilde{E}_z^{i+1/2,j+1/2} = \tilde{E}_z \left( \mathbf{U}_{i+1/2,j+1/2}^{+,+}, \mathbf{U}_{i+1/2,j+1/2}^{-,+}, \mathbf{U}_{i+1/2,j+1/2}^{+,-}, \mathbf{U}_{i+1/2,j+1/2}^{-,-} \right).$$

Here, we employ the two-dimensional HLL flux  $\tilde{E}_z$ , see [14]. Details can be found in Appendix B.

Then, we are able to reconstruct a globally divergence-free magnetic field  $\mathbf{B}_h = (B_{x,h}, B_{y,h}) \in [V_h]^2$  from  $b_x$  and  $b_y$  defined along the interfaces, satisfying

$$(3.11) \quad 1. \quad B_{x,h} \left( x_{i\pm 1/2}^\mp, y \right) = b_x^{i\pm 1/2,j} (y) \quad \text{on } I_{i\pm 1/2,j}^y,$$

$$(3.12) \quad 2. \quad B_{y,h} \left( x, y_{j\pm 1/2}^\mp \right) = b_y^{i,j\pm 1/2} (x) \quad \text{on } I_{i,j\pm 1/2}^x,$$

$$(3.13) \quad 3. \quad \nabla \cdot \mathbf{B}_h = 0 \quad \text{in } K_{ij},$$

for any  $i, j$ . Importantly, to ensure the existence of such reconstruction, the 1D polynomials  $b_x$  and  $b_y$  must satisfy a specific property. Integrating the divergence-free condition (2.3) on cell  $K_{ij}$  and applying Gauss theorem, we get

$$\begin{aligned} 0 &= \int_{K_{ij}} \nabla \cdot \mathbf{B} dx dy = \int_{\partial K_{ij}} \mathbf{B} \cdot \mathbf{n} ds \\ &= \int_{I_{i+1/2,j}^y} B_x dy - \int_{I_{i-1/2,j}^y} B_x dy + \int_{I_{i,j+1/2}^x} B_y dx - \int_{I_{i,j-1/2}^x} B_y dx. \end{aligned}$$

This leads to a necessary condition for  $b_x$  and  $b_y$  [5]

$$(3.14) \quad \Delta y \left( \bar{b}_x^{i+1/2,j} - \bar{b}_x^{i-1/2,j} \right) + \Delta x \left( \bar{b}_y^{i,j+1/2} - \bar{b}_y^{i,j-1/2} \right) = 0,$$

where  $\bar{(\cdot)}$  denotes the cell average. We call (3.14) the *cell-average constraint*. In [5], it is shown that if the cell-average constraint (3.14) holds initially, then the numerical solution of the semi-discrete scheme (3.9)-(3.10) preserves (3.14) at any times.

The detail of the reconstruction procedure will be discussed later.

*Remark 3.7.* Due to the reconstruction of  $\mathbf{B}_h$ , Theorem 3.6 no longer holds. In order to restore the entropy stability, it is important to note that the entropy (2.6) depends only on density and pressure. Hence, a correction step for the total energy  $\mathcal{E}_h$  is needed to ensure that the pressure remains unchanged at each quadrature point. The detail will be provided for fully discrete formulation in Section 4.2.

**3.3. Least-square magnetic field reconstruction.** Now, we discuss the globally divergence-free reconstruction. For simplicity of notation, we will omit the subscript  $i, j$ , and denote the magnetic fields along the interfaces of cell  $K$  as  $b_x^\pm, b_y^\pm$ ,

and the magnetic field inside cell  $K$  as  $\mathbf{B}_h = (B_{x,h}, B_{y,h})$ , which are illustrated in Fig 1. In [29, 14, 5],  $\mathbf{B}_h \in [P^{k+1}(K)]^2$  is reconstructed from the polynomials in  $P^k$  at interfaces. Since we consider  $\mathbf{B}_h \in [Q^{k+1}(K)]^2$  in the nodal DG framework, a new technique based on the least-squares (LS) method is developed to directly compute the nodal values of  $\mathbf{B}_h$ .

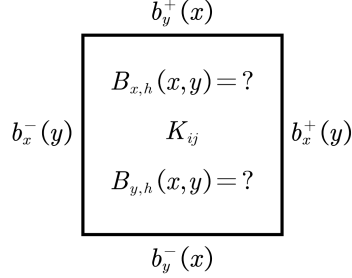


FIG. 1. The notations of the reconstruction problem.

Note that the degrees of approximate polynomials for  $b_x$  and  $b_y$  differ from that for  $\mathbf{B}_h$ . For convenience, we use Legendre basis functions  $\{\phi_l\}_{l=0}^k$  rather than the Lagrange basis at the interface to represent  $b_x^\pm$  and  $b_y^\pm$

$$b_x^\pm(y) = \sum_{l=0}^k b_x^{(l),\pm} \phi_l(Y_j(y)), \quad b_y^\pm(x) = \sum_{l=0}^k b_y^{(l),\pm} \phi_l(X_i(x)),$$

with  $\phi_l$  is the Legendre polynomial of degree  $l$  defined on the reference interval  $[-1, 1]$ . We organize the coefficients as vectors

$$\mathbf{b}_x^\pm = (b_x^{(0),\pm}, \dots, b_x^{(k),\pm})^T, \quad \mathbf{b}_y^\pm = (b_y^{(0),\pm}, \dots, b_y^{(k),\pm})^T.$$

Meanwhile, we also organize the nodal values of  $B_{x,h}$  and  $B_{y,h}$  as vectors

$$\mathbf{B}_x = [B_{x,0,0}, B_{x,1,0}, \dots, B_{x,k+1,k+1}]^T, \quad \mathbf{B}_y = [B_{y,0,0}, B_{y,1,0}, \dots, B_{y,k+1,k+1}]^T,$$

and denote  $\mathbf{B}^{rec} = [\mathbf{B}_x^T, \mathbf{B}_y^T]^T$ . Then, the reconstruction conditions (3.11)-(3.13) are equivalent to the following linear system:

$$(3.15) \quad \begin{bmatrix} (\Delta y / \Delta x) I_{k+2} \otimes D & D \otimes I_{k+2} \\ I_{k+2} \otimes r_0 & O \\ I_{k+2} \otimes l_0 & O \\ O & r_0 \otimes I_{k+2} \\ O & l_0 \otimes I_{k+2} \end{bmatrix} \mathbf{B}^{rec} = \begin{bmatrix} \mathbf{0} \\ V \mathbf{b}_x^+ \\ V \mathbf{b}_x^- \\ V \mathbf{b}_y^+ \\ V \mathbf{b}_y^- \end{bmatrix},$$

where  $l_0 = [1, 0, \dots, 0] \in \mathbb{R}^{k+2}$ ,  $r_0 = [0, \dots, 0, 1] \in \mathbb{R}^{k+2}$ , and the Vandermonde matrix  $V \in \mathbb{R}^{(k+2) \times (k+1)}$  is defined by  $V_{ij} = \phi_j(X_i)$ . It is obvious that there are  $N_d = 2(k+2)^2$  unknowns for  $\mathbf{B}^{rec}$ . However, there are only  $(k+2)^2 - 1 + 4(k+1)$  linearly independent conditions in (3.15). Furthermore, the cell-average constraint (3.14) reduces the number of conditions by one [5]. Thus, the total number of linearly independent conditions is given by

$$N_c = 4(k+1) + (k+2)^2 - 2.$$

Since  $N_d \geq N_c$  for any  $k \in \mathbb{N}$ , the reconstruction exists but may lack uniqueness. Note that if we require  $b_x, b_y \in P^{k+1}$ , it is possible that  $N_c > N_d$ , which would result in the reconstruction not existing. This explains why the degree of the approximate polynomials for  $b_x$  and  $b_y$  is chosen to be  $k$  rather than  $k+1$ .

To construct the reconstruction uniquely, we employ the least-squares method. Denote (3.15) as

$$(3.16) \quad A\mathbf{B}^{rec} = \mathbf{b},$$

and the magnetic field inside cell  $K$  before reconstruction as  $\tilde{\mathbf{B}}$ . Then  $\mathbf{B}^{rec}$  is obtained by solving the following constrained optimization problem

$$(3.17) \quad \min_{\mathbf{B}} \left\| \mathbf{B} - \tilde{\mathbf{B}} \right\|_{M_2}^2, \quad \text{s.t. } A\mathbf{B} = \mathbf{b},$$

where

$$\|\mathbf{X}\|_{M_2}^2 = \mathbf{X}^T M_2 \mathbf{X}, \quad M_2 = \begin{bmatrix} M \otimes M & O \\ O & M \otimes M \end{bmatrix}.$$

Assume the singular value decomposition of  $A$  is  $A = USV^T$ , then (3.16) can be written as  $SV^T\mathbf{B}^{rec} = U^T\mathbf{b}$ . By removing the zero rows from the above system, we obtain an equivalent system with full row rank

$$A_1\mathbf{B}^{rec} = \mathbf{b}_1.$$

Lastly,  $\mathbf{B}^{rec}$  is computed by solving the following system

$$(3.18) \quad \begin{bmatrix} M_2 & A_1^T \\ A_1 & O \end{bmatrix} \begin{bmatrix} \mathbf{B}^{rec} \\ \boldsymbol{\lambda} \end{bmatrix} = \begin{bmatrix} M_2 \tilde{\mathbf{B}} \\ \mathbf{b}_1 \end{bmatrix},$$

where  $\boldsymbol{\lambda}$  is the Lagrangian multiplier. Since  $A_1$  is a full row-rank matrix, the above system (3.18) has a unique solution. A more detailed discussion is given in Appendix D.

#### 4. Limiting strategy and fully discrete formulation.

**4.1. Limiting strategy.** As mentioned in [15], entropy stable schemes offer enhanced robustness. However, for problems involving strong shocks, a nonlinear limiter is still required to suppress spurious oscillations. The main challenge lies in ensuring that entropy does not increase after applying the limiter. Many existing limiters such as the popular TVB limiter with characteristic decomposition cannot guarantee this property [42]. To address the difficulty, we recall the following lemma in [15].

LEMMA 4.1. *Suppose  $\omega_j > 0$  for  $1 \leq j \leq N$  with  $\sum_{j=1}^N \omega_j = 1$ . Define the average*

$$\bar{\mathbf{U}} = \sum_{j=1}^N \omega_j \mathbf{U}_j \text{ and the rescaled values towards the average}$$

$$\tilde{\mathbf{U}}_j = \bar{\mathbf{U}} + \theta(\mathbf{U}_j - \bar{\mathbf{U}}), \quad j = 1, \dots, N, \quad 0 \leq \theta \leq 1.$$

Then, for any convex function  $\mathcal{U}$ , we have

$$\sum_{j=1}^N \omega_j \mathcal{U}(\tilde{\mathbf{U}}_j) \leq \sum_{j=1}^N \omega_j \mathcal{U}(\mathbf{U}_j).$$

The theorem ensures that rescaling

$$\tilde{\mathbf{U}}_{i_1, j_1}^{i, j} = \bar{\mathbf{U}}^{i, j} + \theta_{ij}(\mathbf{U}_{i_1, j_1}^{i, j} - \bar{\mathbf{U}}^{i, j}), \quad 0 \leq i_1, j_1 \leq k+1$$

by the same parameter  $0 \leq \theta_{ij} \leq 1$  will not increase the discrete entropy of a cell. Inspired by the oscillation-free DG method [43] and its subsequent works [48, 57], we employ a similar strategy to determine the parameter  $\theta_{ij}$  by measuring the jump intensity of the numerical solution as well as its derivatives at interfaces. Specifically,  $\theta_{ij}$  is given by

$$(4.1) \quad \theta_{ij} = \exp(-\sigma_{ij}\Delta t), \quad \sigma_{ij} = \max_{1 \leq m \leq 8} \sigma_{ij}^{(m)},$$

where  $\Delta t$  denotes the time step and

$$\sigma_{ij}^{(m)} = c_{f, ij} \sqrt{\Delta x \Delta y} \sum_{l=0}^{k+1} \sum_{l_1+l_2=l} l(l+1) \Delta x^{l_1} \Delta y^{l_2} \left\| \left[ \left[ D_x^{l_1} D_y^{l_2} u^{(m), i, j} \right] \right] \right\|_{\partial K_{ij}},$$

with  $D_x = I_{k+2} \otimes D$ ,  $D_y = D \otimes I_{k+2}$ ,  $u^{(m)}$  being the  $m$ -th component of  $\mathbf{U}$  and  $\|[\![\cdot]\!]\|_{\partial K_{ij}}$  representing the jump across the cell boundary

$$\begin{aligned} \|[\![u]\!]\|_{\partial K_{ij}} = & \sum_{i_1=0}^{k+1} \omega_{i_1} \left( \left| u_{0, i_1}^{i, j} - u_{k+1, i_1}^{i-1, j} \right| + \left| u_{0, i_1}^{i+1, j} - u_{k+1, i_1}^{i, j} \right| \right. \\ & \left. + \left| u_{i_1, 0}^{i, j} - u_{i_1, k+1}^{i, j-1} \right| + \left| u_{i_1, 0}^{i, j+1} - u_{i_1, k+1}^{i, j} \right| \right). \end{aligned}$$

For the parameter  $c_f$ , we set

$$c_{f, ij} = \frac{c_0}{4k(k+1)} \max_{i_1, j_1} \left\{ \frac{1}{H_{i_1, j_1}^{i, j}} \right\}, \quad H = \frac{\mathcal{E} + p^*}{\rho},$$

where  $c_0 > 0$  is a free-parameter.

In addition, we need to apply a limiter to the magnetic field on interfaces to ensure the globally divergence-free property. For example, for the magnetic field  $b_x$  at interface  $\Gamma_{i+1/2, j}^y$ , we propose limiting its high-order moments using  $\theta_{ij}$  in its adjacent cells, while keeping the average unchanged. Specifically, we set

$$\tilde{b}_x^{(l)} = \theta_{i+1/2, j} b_x^{(l)}, \quad \text{for } l = 1, \dots, k,$$

with  $\theta_{i+1/2, j} = \min\{\theta_{ij}, \theta_{i+1, j}\}$ .  $b_y$  is limited similarly. Then, the interior magnetic field is reconstructed from  $\tilde{b}_x$  and  $\tilde{b}_y$ . Note that the limiting of  $b_x$  and  $b_y$  will preserve the discrete entropy in each cell through an energy correction, which will be introduced later. Furthermore, since the limiter also maintains the cell averages, the cell-average constraint (3.14) remains satisfied. Hence, we can reconstruct a globally divergence-free magnetic field without spurious oscillations.

**4.2. The fully discrete ES-GDF framework.** For time discretization, we employ the 10-stage 4th-order strong stability-preserving Runge-Kutta (SSP-RK4) scheme described in [38]. For illustrative purposes, we present the algorithm flowchart for the proposed ES-GDF scheme coupled with the forward Euler method to update the solution from time  $t^n$  to  $t^{n+1} = t^n + \Delta t$ . This approach can be easily extended to the SSP-RK4 time discretization.

**Step 1** Update the numerical solution in cells based on the nodal DG scheme (3.1) and obtain  $\tilde{\mathbf{U}}^{n+1} = (\tilde{\rho}, \tilde{\rho}\mathbf{u}, \tilde{\mathcal{E}}, \tilde{\mathbf{B}})^T$ .

**Step 2** Update the magnetic field  $\tilde{b}_x^{n+1}$  and  $\tilde{b}_y^{n+1}$  on the interfaces based on (3.9)-(3.10).

**Step 3** Apply the limiter to  $\tilde{b}_x^{n+1}, \tilde{b}_y^{n+1}$  on the interfaces and  $\tilde{\mathbf{U}}^{n+1}$  in cells to obtain  $(b_x^{n+1}, b_y^{n+1})$  and  $\mathbf{U}^{*,n+1} = (\rho_h^{n+1}, (\rho\mathbf{u})_h^{n+1}, \mathcal{E}_h^*, \mathbf{B}_h^*)^T$ .

**Step 4** Reconstruct the internal magnetic field  $\mathbf{B}^{n+1}$  using  $b_x^{n+1}, b_y^{n+1}$ , and correct the total energy  $\mathcal{E}^{n+1}$ . Moreover, in order to maintain the discrete entropy, we also adjust the energy to ensure that the pressure remains unchanged,

$$(4.2) \quad \mathcal{E}_h^{n+1} = \mathcal{E}_h^* + \frac{1}{2} \left( \|\mathbf{B}_h^{n+1}\|^2 - \|\mathbf{B}_h^*\|^2 \right),$$

at each Gauss-Lobatto point. Finally, we can obtain

$$\mathbf{U}_h^{n+1} = (\rho_h^{n+1}, (\rho\mathbf{u})_h^{n+1}, \mathcal{E}_h^{n+1}, \mathbf{B}_h^{n+1})^T.$$

*Remark 4.2.* The key step the ES-GDF DG framework is the correction procedure (4.2) in **Step 4**. Note that if we simply set  $\mathcal{E}_h^{n+1} = \mathcal{E}_h^*$ , the change in the magnetic field would lead to a corresponding change in pressure, and there would be no guarantee that

$$\mathcal{U}^{tot}((\rho_h^{n+1}, (\rho\mathbf{u})_h^{n+1}, \mathcal{E}_h^*, \mathbf{B}_h^{n+1})^T) \leq \mathcal{U}^{tot}(\mathbf{U}^{*,n+1}).$$

Here,  $\mathcal{U}^{tot}(\mathbf{U}_h)$  denotes the discrete total entropy of  $\mathbf{U}_h$  on  $\Omega$ . Note that this treatment will result in the loss of local energy conservation. Meanwhile, the corresponding conservation error in each cell  $K_{ij}$  is associated with changes in the magnetic energy density due to the reconstruction:

$$\bar{\mathcal{E}}^{n+1,i,j} - \bar{\mathcal{E}}^{*,i,j} = \sum_{i_1,j_1=0}^{k+1} \frac{1}{8} \omega_{i_1} \omega_{j_1} \left( \|\mathbf{B}_{i_1,j_1}^{n+1,i,j}\|^2 - \|\mathbf{B}_{i_1,j_1}^{*,i,j}\|^2 \right).$$

Thus, as long as the proposed reconstruction procedure maintains high-order accuracy, the conservative error of  $\mathcal{E}$  is also high-order accurate [6]. Furthermore, we may add an additional constraint to the optimization problem (3.17) to ensure the local magnetic energy is conserved, hence preserving the local total energy conservation. However, it is nontrivial to rigorously show that the admissible set is nonempty. We will leave the investigation for future work.

**5. Numerical experiments.** In this section, we simulate the ideal MHD equation to verify the accuracy and efficiency of our scheme. We use the time step

$$\Delta t = \frac{\text{CFL}}{\alpha_x/\Delta x + \alpha_y/\Delta y}, \quad \text{CFL} = 0.45$$

for all tests. Here,  $\alpha_x = \max |\lambda(\partial \mathbf{F}/\partial \mathbf{U})|$ ,  $\alpha_y = \max |\lambda(\partial \mathbf{G}/\partial \mathbf{U})|$ , and  $\lambda(\cdot)$  is the eigenvalue of the matrix. We use uniform meshes for convenience. To compare the performance of the schemes, we denote “ES-GDF” as our proposed scheme, and “ES” as the original entropy stable nodal DG scheme designed in [42]. Without special declaration, we only present the results of  $k = 2$ . For the example containing strong shock, the limiter introduced in Section 4.1 will be used.

*Example 5.1* (Smooth MHD vortex). First, we consider the MHD vortex problem, which is originally introduced by Shu [53] in the hydrodynamical system, and was

extended to MHD equations by Balsara [3]. Here we use the same setup in [39]. We use a uniform mesh with  $N = N_x = N_y$ . In Table 1, we present the  $L^2$  errors and orders of the numerical solution with  $k = 1, 2, 3$  at  $T = 20$ , when the exact solution coincides with the initial data. It can be seen that our schemes also maintain the designed accuracy. In Fig 1, we plot the time evolution of the absolute values of relative deviation in the conservative variables for ES-GDF and ES schemes on  $N_x \times N_y = 64 \times 64$  and  $N_x \times N_y = 128 \times 128$  meshes with  $k = 2$ . We recall that both two schemes are conservative in density. Hence, we only plot momentum, total energy, and magnetic field here (denoted by “mom”, “ene”, and “mag”). The error of momentum and magnetic field is calculated in  $L^1$  vector norm. It is observed that both schemes are not conservative in total energy, and the errors are at the same level. However, for momentum and magnetic field, the proposed ES-GDF scheme maintains the conservation errors at machine accuracy, while the ES scheme shows non-conservation.

TABLE 1  
Example 5.1: Smooth MHD vortex. The  $L^2$  errors and orders at final time  $T = 20$ .

$N$	$\rho$	order	$\rho u_x$	order	$B_x$	order	$\mathcal{E}$	order
$k = 1$								
32	3.14e-04	–	1.51e-03	–	4.87e-03	–	2.47e-03	–
64	9.62e-05	1.71	2.23e-04	2.76	9.93e-04	2.29	4.40e-04	2.49
128	1.69e-05	2.51	3.69e-05	2.60	1.50e-04	2.72	7.39e-05	2.57
256	3.03e-06	2.48	7.55e-06	2.29	2.54e-05	2.57	1.45e-05	2.35
$k = 2$								
32	3.02e-05	–	5.82e-05	–	1.36e-04	–	9.80e-05	–
64	3.49e-06	3.11	3.83e-06	3.92	1.39e-05	3.29	9.05e-06	3.44
128	3.28e-07	3.41	3.47e-07	3.46	2.13e-06	2.71	9.17e-07	3.30
256	3.85e-08	3.09	4.24e-08	3.03	2.84e-07	2.91	1.11e-07	3.05
$k = 3$								
32	1.96e-06	–	2.59e-06	–	7.29e-06	–	5.58e-06	–
64	1.49e-07	3.72	1.55e-07	4.06	4.29e-07	4.09	3.68e-07	3.92
128	5.49e-09	4.76	6.22e-09	4.64	2.65e-08	4.02	1.44e-08	4.68
256	2.48e-10	4.47	3.35e-10	4.21	1.65e-09	4.00	7.14e-10	4.33

Example 5.2 (Rotated shock tube). We consider a 2D Riemann problem obtained by rotating the one-dimensional Brio-Wu shock tube [10] with an angle  $\alpha = \arctan(0.5)$ . We want to remark that in this problem, the constancy of the parallel component  $B_{||} := B_x \cos \alpha + B_y \sin \alpha$  is difficult to obtain in numerical schemes which do not satisfy the discrete divergence-free property. The computational domain is  $\Omega = [0, 1] \times [(2/N_x) \cot \alpha]$ . The Dirichlet boundary conditions are applied to the left and right boundaries according to the initial condition. The top and bottom boundaries are imposed with the shifted periodic type according to the translational symmetry, as detailed in [56]. The “exact” solution is computed by a classical third-order one-dimensional DG scheme using TVB limiter with  $M = 1$  on 10,000 cells for the non-rotated version, which can be treated as a one-dimensional problem. The

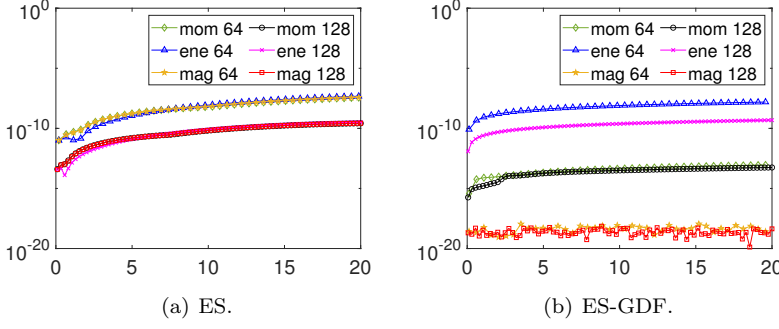


FIG. 1. *Example 5.1: Smooth MHD vortex. Time evolution of the absolute values of relative deviation in the conservative variables on different meshes for  $k = 2$ .*

initial data is given by

$$(\rho, u_x, u_y, u_z, B_x, B_y, B_z, p) = \begin{cases} \left(1, 0, 0, 0, \frac{0.5}{\sqrt{5}}, \frac{2.75}{\sqrt{5}}, 0, 1\right), & 2x + y < 1, \\ \left(0.125, 0, 0, 0, \frac{2.5}{\sqrt{5}}, \frac{-1.25}{\sqrt{5}}, 0, 0.1\right), & 2x + y \geq 1. \end{cases}$$

Notably, without the entropy stable treatment, both the standard nodal DG scheme and GDF nodal DG scheme will break down in the first several steps. In Fig 2, we present the result at  $T = 0.1 \cos \alpha = 0.2/\sqrt{5}$  on  $N_x \times N_y = 512 \times 2$  meshes without limiter. It is clear that the ES-GDF DG scheme produces a more stable result, while the ES DG scheme appears unstable in the range  $0.45 < x < 0.62$ . This may be caused by the non-constancy of  $B_{||}$ . The results with the limiter is shown in Fig 3, we can see the ES-GDF DG scheme gives a more compatible simulation, especially for  $B_{||}$ .

*Example 5.3 (Magnetic field loop).* We consider the magnetic field loop problem, which is first introduced in [31], and our setup is the same as in [40]. This test involves the advection of magnetic field loop over a periodic domain. The magnetic field will transport over the domain and return to its initial position at positive integer times. This problem can be computed without any limiter with ES treatment. In Fig 4, we present the result of  $\sqrt{B_x^2 + B_y^2}$  at  $T = 2$  on  $N_x \times N_y = 240 \times 120$  meshes. Here, we also compare it with the ES DG scheme [42], showing that the ES-GDF scheme better captures the features of the solution. In Fig 5, we present the evolution of total entropy and divergence over time, where the divergence is defined as [19]

$$\|\text{div} \mathbf{B}\| = \sum_{K \in \mathcal{K}} \left( \int_K |\nabla \cdot \mathbf{B}| \, dx dy + \int_{\partial K} \|[\mathbf{B} \cdot \mathbf{n}]\| \, ds \right).$$

It can be seen that the entropy is non-increasing over time, and the total divergence of the magnetic field closes to machine error.

*Example 5.4 (Kelvin-Helmholtz instability).* We consider the Kelvin-Helmholtz instability problem and follow the setup in [46]. This instability has been widely studied in the literature, and it clearly shows the advantages of maintaining a divergence-free magnetic field. The ES-GDF DG scheme can simulate this problem without any limiters, while the non-ES DG schemes and the ES DG scheme without GDF treatment will blow up if the limiter is not applied.

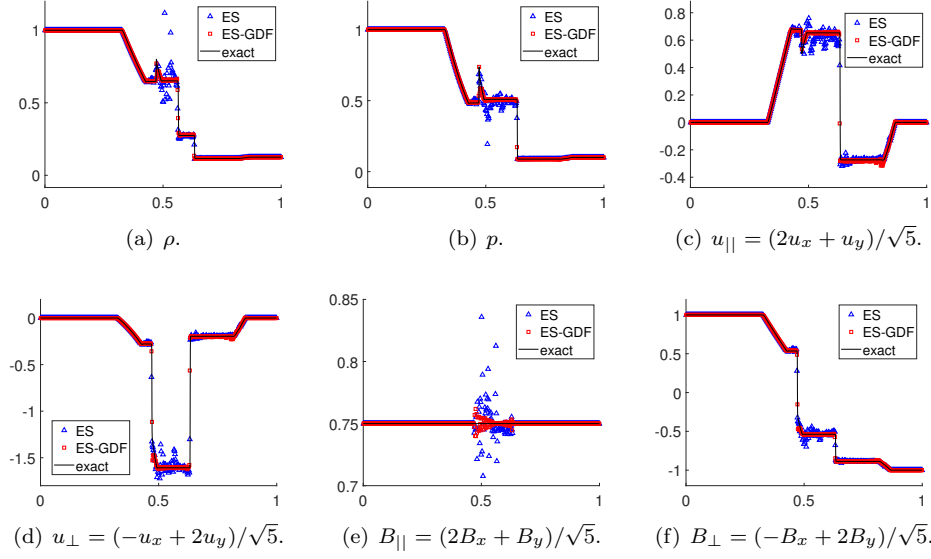


FIG. 2. *Example 5.2: The rotated shock tube. The numerical solution at  $T = 0.2/\sqrt{5}$  on  $N_x \times N_y = 512 \times 2$  meshes. No limiter is applied.*

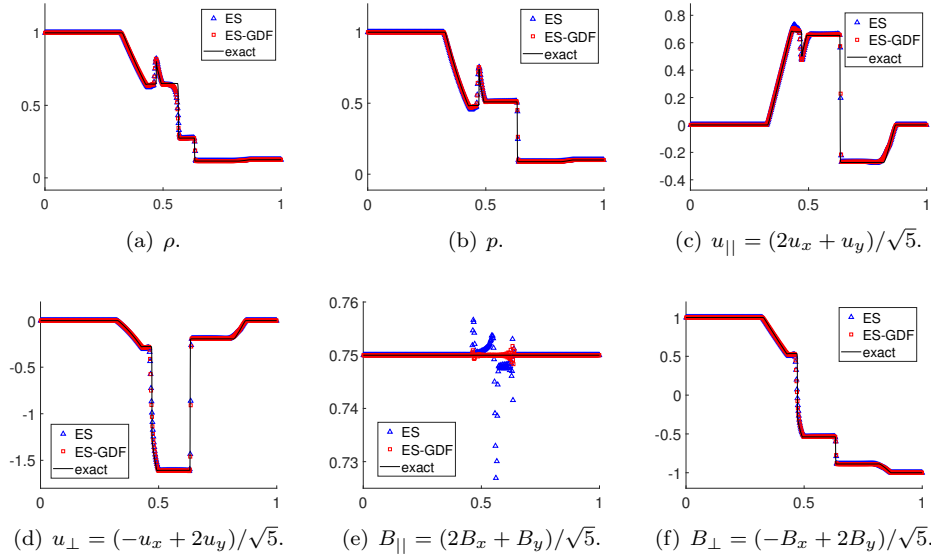


FIG. 3. *Example 5.2: The rotated shock tube. The numerical solution at  $T = 0.2/\sqrt{5}$  on  $N_x \times N_y = 512 \times 2$  meshes with the limiter.*

We simulate this problem on mesh with  $N_x \times N_y = 256 \times 512$  and the results of  $B_p/B_t$  at  $T = 5, 12, 20$  with  $k = 1, 2, 3$  are shown in Fig 6, where  $B_p = \sqrt{B_x^2 + B_y^2}$ ,  $B_t = B_z$ . In Fig 7, we plot the evolution of the poloidal magnetic energy



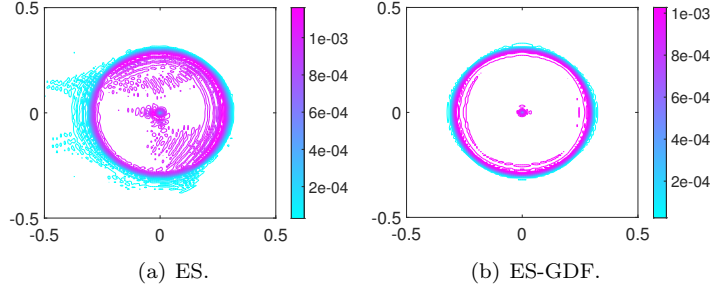


FIG. 4. *Example 5.3: Magnetic field loop.* The numerical solution of  $\sqrt{B_x^2 + B_y^2}$  at  $T = 2$  on  $N_x \times N_y = 240 \times 120$  meshes with 40 contour lines. No limiter is applied.

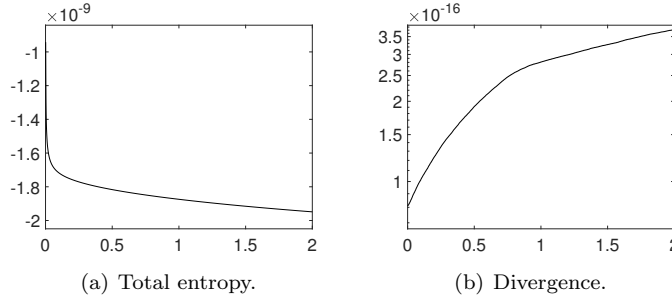


FIG. 5. *Example 5.3: Magnetic field loop.* The time evolution of total entropy and divergence norm on  $N_x \times N_y = 240 \times 120$  meshes. No limiter is applied.

$\langle B_p^2 \rangle$  with different  $k$  and meshes, where

$$\langle B_p^2(t) \rangle = \left( \int_{\Omega} B_p^2(t) \, dx dy \right) / \left( \int_{\Omega} B_p^2(0) \, dx dy \right).$$

For  $t \leq 5$ , the perturbation follows a linear growth phase during which magnetic field lines wound up through the formation of a typical cat's eye vortex structure [45, 37]. When  $t \geq 8$ , field amplification is eventually prevented by tearing mode instabilities, leading to reconnection events capable of expelling magnetic flux from the vortex [45]. One can clearly see that small-scale structures are captured well with the proposed ES-GDF scheme. Further, we can see the poloidal magnetic energy grows faster in the transition to turbulence when a higher-order scheme is selected. This indicates that the overall numerical dissipation is smaller for higher-order scheme. The evolution of total entropy and divergence are shown in Fig 8, indicating that the entropy is non-increase for reflective walls.

*Example 5.5 (Rotor).* This benchmark test problem is first introduced in [6], and we follow the setup in [56]. It describes the spinning of a dense rotating disc of fluid in the center while ambient fluid is at rest. The magnetic field wraps around the rotating dense fluid turning it into an oblate shape. If the numerical scheme does not sufficiently control the divergence error in the magnetic field, distortion can be observed in Mach number [39]. For this problem, the limiter is applied.

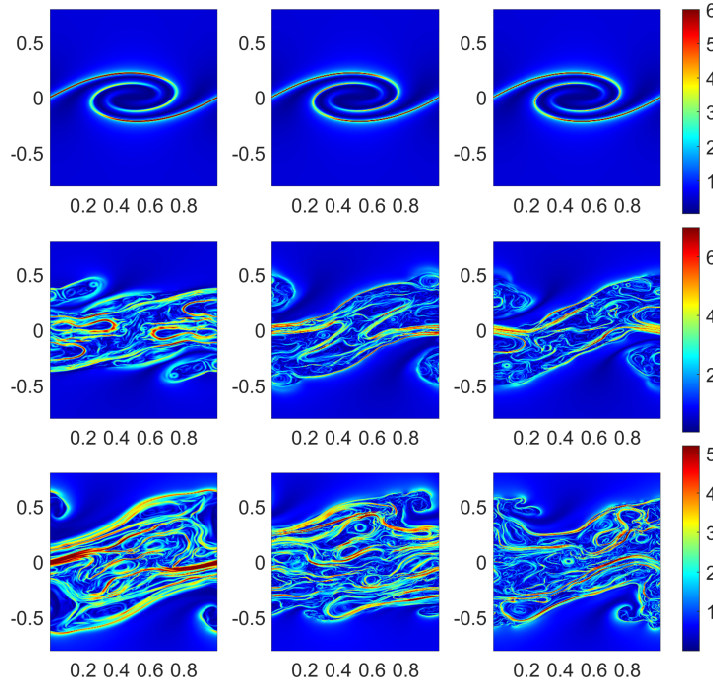


FIG. 6. *Example 5.4: Kelvin-Helmholtz instability. The numerical solution of  $B_p/B_t$  on  $N_x \times N_y = 256 \times 512$  meshes. From top to bottom:  $T = 5, 12, 20$ ; from left to right:  $k = 1, 2, 3$ . No limiter is applied.*

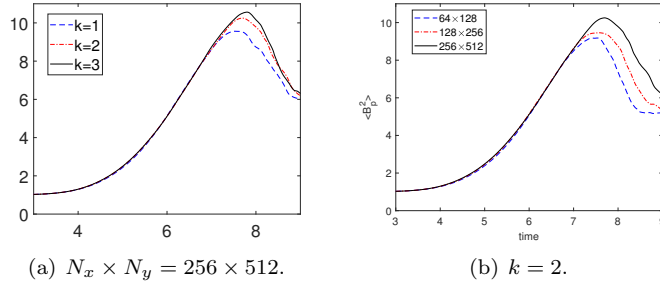


FIG. 7. *Example 5.4: Kelvin-Helmholtz instability. The time evolution of  $\langle B_p^2 \rangle$  with different  $k$  and meshes. No limiter is applied.*

In Fig 9, we present the results of Mach number in the central area at  $T = 0.295$  on different meshes, and no distortion is obtained. In Fig 10, we plot the conservative errors of ES-GDF and ES scheme. In Fig 11, we present the evolution of total entropy and divergence over time with  $N_x \times N_y = 400 \times 400$ . It can be seen that our scheme conserves the momentum and magnetic field, dissipates the entropy, and maintains the globally divergence-free property for discontinuous problems.

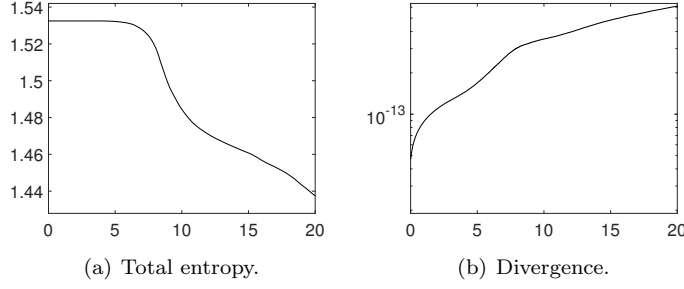


FIG. 8. *Example 5.4: Kelvin-Helmholtz instability.* The time evolution of total entropy and divergence norm with time on mesh with  $N_x \times N_y = 256 \times 512$  for  $k = 2$ . No limiter is applied.

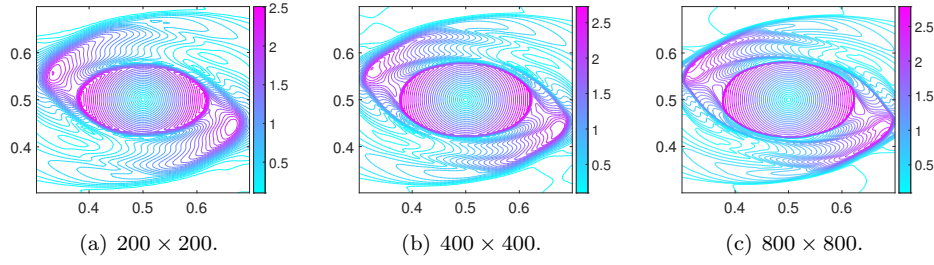


FIG. 9. *Example 5.5: Rotor.* The Mach number of the central area at  $T = 0.295$  with different meshes. 30 contour lines are used.

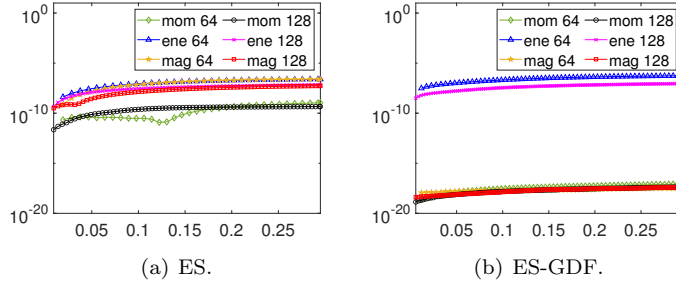


FIG. 10. *Example 5.5: Rotor.* The conservative errors for momentum, total energy, and magnetic field on different meshes.

*Example 5.6 (MHD blast).* We consider the MHD blast problem [6]. This is a challenging test problem and is often used as a benchmark for testing the robustness of the numerical algorithms in terms of maintaining positivity of solutions. The fluid pulse has very small plasma beta about  $2.51 \times 10^{-4}$ . For this problem, the limiter is applied. The result at  $T = 0.01$  on mesh with  $N_x \times N_y = 200 \times 200$  is shown in Fig 12. Compared to the results in [29], even without adding positivity limiters, we obtain non-negative pressure at all time layers, where the minimum pressure at final time is

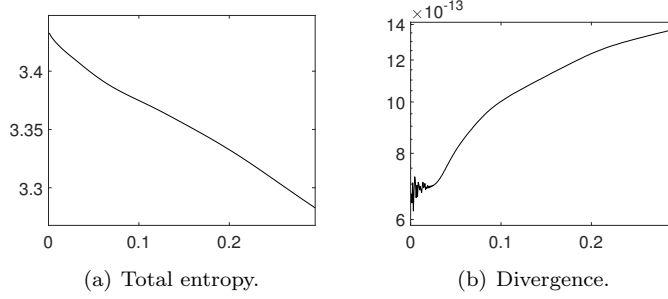


FIG. 11. *Example 5.5: Rotor. The development of total entropy and divergence norm with time on  $N_x \times N_y = 400 \times 400$  meshes.*

about 0.0952. This may indicate that entropy stability can enhance computational stability for this problem.

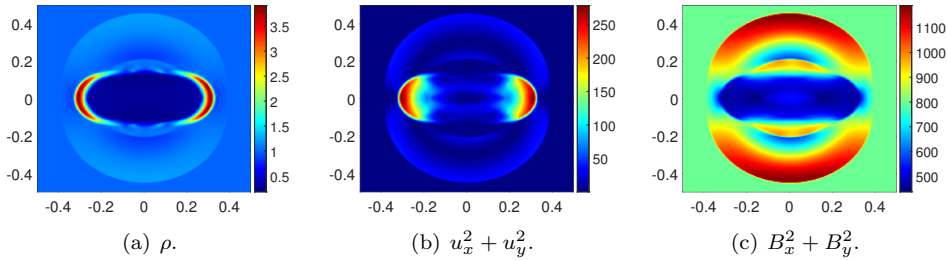


FIG. 12. *Example 5.6: MHD blast. The numerical solution at  $T = 0.01$  with  $N_x \times N_y = 200 \times 200$ .*

*Example 5.7 (Cloud shock interaction).* Finally, we consider the cloud shock problem [51], and use the same setup in [17]. This problem simulates an MHD shock propagating toward a stationary bubble. After the shock passes through the bubble, very complex structures will appear in the computational domain. Those structures around the bubble are susceptible to numerical dissipations and low dissipative schemes are advantageous to obtain less smeared structures. In this problem, the limiter is applied. In Fig 13, we present the results at  $T = 0.06$  with  $600 \times 600$ . It can be seen that the ES-GDF DG scheme resolves shocks and other complex features very well without introducing negative pressure, indicates the low-dissipation and robustness of our scheme. The solution matches well with the results in the literature, such as those in [17, 58, 16].

**6. Concluding remarks.** In this paper, we present a globally divergence-free entropy stable nodal DG method that directly solves the conservative form of ideal MHD equation. By using the constraint-preserving schemes [5] to update the magnetic field at interfaces, we can obtain the globally divergence-free internal magnetic field by a novel least-square reconstruction, where  $Q^{k+1}$  basis is used. Utilizing the SBP property of stiffness matrix, we are able to prove the entropy stability of semi-discrete scheme. For problems containing strong shock, we propose a new limiting strategy, which can control the numerical oscillation and preserve the divergence-free property.

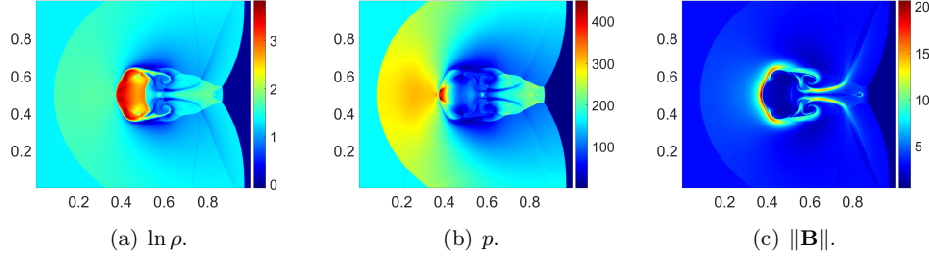


FIG. 13. *Example 5.7: Cloud shock interaction. The numerical solution at  $T = 0.06$  with  $N_x \times N_y = 600 \times 600$ .*

And employing a energy correction step, we can guarantee the total entropy will not increase. Numerical results verify that our scheme can achieve the designed accuracy, dissipate the entropy, and control the divergence norm at machine error level. Future works may include the extension to unstructured meshes, and the application of other equations.

## Appendix A. Entropy conservative flux and entropy stable flux.

**A.1. Entropy conservative flux.** For the MHD equations, Chandrashekar and Klingenberg [13] suggested the following entropy conservative flux:

$$\begin{aligned}
 \mathbf{F}_1^S &= \hat{\rho} \bar{u}_x, \\
 \mathbf{F}_2^S &= \frac{\bar{\rho}}{2\bar{\beta}} + \bar{u}_x \mathbf{F}_1^S + \frac{1}{2} \overline{\|\mathbf{B}\|^2} - \bar{B}_x \bar{B}_x, \\
 \mathbf{F}_3^S &= \bar{u}_y \mathbf{F}_1^S - \bar{B}_x \bar{B}_y, \\
 \mathbf{F}_4^S &= \bar{u}_z \mathbf{F}_1^S - \bar{B}_x \bar{B}_z, \\
 \mathbf{F}_6^S &= 0, \\
 \mathbf{F}_7^S &= \frac{1}{\bar{\beta}} (\bar{\beta} \bar{u}_x \bar{B}_y - \overline{\beta u_y B_x}), \\
 \mathbf{F}_8^S &= \frac{1}{\bar{\beta}} (\bar{\beta} \bar{u}_x \bar{B}_z - \overline{\beta u_z B_x}), \\
 \mathbf{F}_5^S &= \frac{1}{2} \left[ \frac{1}{(\gamma - 1) \hat{\beta}} - \overline{\|\mathbf{u}\|^2} \right] \mathbf{F}_1^S + \bar{u}_x \mathbf{F}_2^S + \bar{u}_y \mathbf{F}_3^S + \bar{u}_z \mathbf{F}_4^S \\
 &\quad + \bar{B}_x \mathbf{F}_6^S + \bar{B}_y \mathbf{F}_7^S + \bar{B}_z \mathbf{F}_8^S - \frac{1}{2} \bar{u}_x \overline{\|\mathbf{B}\|^2} + (\bar{u}_x \bar{B}_x + \bar{u}_y \bar{B}_y + \bar{u}_z \bar{B}_z) \bar{B}_x,
 \end{aligned}$$

where  $\overline{(a, b)} = (a + b)/2$  is the arithmetic average, and  $\hat{(\cdot)}$  is the logarithmic average of two strictly positive quantities as

$$\hat{\alpha} = \frac{\alpha_r - \alpha_l}{\ln \alpha_r - \ln \alpha_l}.$$

The formula of  $\mathbf{G}^S$  is similar.

**A.2. Entropy stable flux.** For entropy stable fluxes, it is well known that the Godunov flux based on exact Riemann solvers is by definition entropy stable. Meanwhile, many approximate Riemann solvers, such as the HLL or Lax–Friedrichs

fluxes are also entropy stable if the estimates of left and right local wave speed  $S_L$ ,  $S_R$  satisfy  $S_L \leq S_L^{real}$ ,  $S_R \geq S_R^{real}$ , where  $S_{L,R}^{real}$  are the real minimal and maximal wave speed of the Riemann problem at the interface [15]. In particular, the HLL flux is given by

$$\hat{\mathbf{F}}^{HLL}(\mathbf{U}_L, \mathbf{U}_R) = \begin{cases} \mathbf{F}(\mathbf{U}_L), & S_L \geq 0, \\ \frac{S_R \mathbf{F}_L - S_L \mathbf{F}_R + S_R S_L (\mathbf{U}_R - \mathbf{U}_L)}{S_R - S_L}, & S_L < 0 < S_R, \\ \mathbf{F}(\mathbf{U}_R), & S_R \leq 0, \end{cases}$$

If we denote the non-positive part of  $S_L$  by  $\mathcal{S}_L = \min\{S_L, 0\}$ , and the non-negative part of  $S_R$  by  $\mathcal{S}_R = \max\{S_R, 0\}$ , then the HLL flux can be written by

$$(A.1) \quad \hat{\mathbf{F}}^{HLL}(\mathbf{U}_L, \mathbf{U}_R) = \frac{\mathcal{S}_R \mathbf{F}_L - \mathcal{S}_L \mathbf{F}_R + \mathcal{S}_R \mathcal{S}_L (\mathbf{U}_R - \mathbf{U}_L)}{\mathcal{S}_R - \mathcal{S}_L}.$$

However, the computation of  $S_L$  and  $S_R$  is non-trivial. To address this, Toro recommends the two-rarefaction approximate in [?], then Guermond and Popov [?] prove that the two-rarefaction approximated wave speeds indeed provide the correct bounds for Euler equations with  $1 < \gamma \leq 5/3$ . However, for MHD system, the Riemann problem becomes more complex and is difficult to analyze. In [7, 8], another “relaxation” approach is used, and the 3-wave and 7-wave approximate Riemann solver are designed, which are proved to be entropy stable. Further, if we simply use the HLL solver (A.1), but the wavespeeds  $S_L$ ,  $S_R$  are chosen by the above 3-wave solver, then it is also entropy stable [8].

Specifically, for two given state  $\mathbf{U}_L, \mathbf{U}_R$ , the explicit formula of  $S_L(\mathbf{U}_L, \mathbf{U}_R)$  and  $S_R(\mathbf{U}_L, \mathbf{U}_R)$  along  $x$ -direction are given by

$$S_L = u_L - \mathcal{C}_L, \quad S_R = u_R + \mathcal{C}_R,$$

where

$$\begin{aligned} \mathcal{C}_L &= c_{f,L}^0 + \alpha \left( (u_L - u_R)_+ + \frac{(p_R - p_L)_+}{\rho_L c_{f,L} + \rho_R c_{f,R}} \right), \\ \mathcal{C}_R &= c_{f,R}^0 + \alpha \left( (u_L - u_R)_+ + \frac{(p_R - p_L)_+}{\rho_L c_{f,L} + \rho_R c_{f,R}} \right), \\ c_{f,L}^0 &= \left\{ \frac{1}{2} \left( a_L + \frac{\|\mathbf{B}_L\|^2}{\rho_L x_L} + \sqrt{\left( a_L + \frac{\|\mathbf{B}_L\|^2}{\rho_L x_L} \right)^2 - 4a_L \frac{B_{x,L}^2}{\rho_L x_L}} \right) \right\}^{1/2}, \\ c_{f,R}^0 &= \left\{ \frac{1}{2} \left( a_R + \frac{\|\mathbf{B}_R\|^2}{\rho_R x_R} + \sqrt{\left( a_R + \frac{\|\mathbf{B}_R\|^2}{\rho_R x_R} \right)^2 - 4a_R \frac{B_{x,R}^2}{\rho_R x_R}} \right) \right\}^{1/2}, \end{aligned}$$

and

$$\begin{aligned} X_L &= \frac{1}{c_{f,L}} \left[ (u_L - u_R)_+ + \frac{(p_R - p_L)_+}{\rho_L c_{f,L} + \rho_R c_{f,R}} \right], \\ X_R &= \frac{1}{c_{f,R}} \left[ (u_L - u_R)_+ + \frac{(p_R - p_L)_+}{\rho_L c_{f,L} + \rho_R c_{f,R}} \right], \\ x_L &= 1 - \frac{X_L}{1 + \alpha X_L}, \quad x_R = 1 - \frac{X_R}{1 + \alpha X_R} \end{aligned}$$

with  $a = \sqrt{\gamma p / \rho}$ ,  $\alpha = (\gamma + 1)/2$ ,  $(\cdot)_+ = \max\{\cdot, 0\}$ , and  $c_{f,L}, c_{f,R}$  denotes the largest eigenvalue of  $\partial \mathbf{F}(\mathbf{U}) / \partial \mathbf{U}$  at  $\mathbf{U} = \mathbf{U}_L, \mathbf{U}_R$ , respectively.

### Appendix B. Two-dimensional HLL Riemann solver.

For four given states at a vertex  $\Lambda$ , the two-dimensional HLL flux  $\tilde{E}_z|_\Lambda = \tilde{E}_z(\mathbf{U}_{LD}, \mathbf{U}_{LU}, \mathbf{U}_{RD}, \mathbf{U}_{RU})$  is calculated by following [14]. To help with the presentation, we illustrate the notations of states around a vertex  $\Lambda$  in Fig 14.

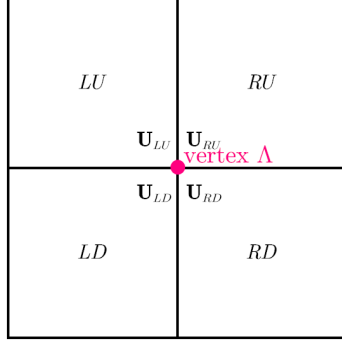


FIG. 14. The notations around a vertex  $\Lambda$ .

First, the wave speeds are chosen by

$$\begin{aligned} S_R|_\Lambda &= \max\{S_R(\mathbf{U}_{LU}, \mathbf{U}_{RU}), S_R(\mathbf{U}_{LD}, \mathbf{U}_{RD})\}, \\ S_L|_\Lambda &= \min\{S_L(\mathbf{U}_{LU}, \mathbf{U}_{RU}), S_L(\mathbf{U}_{LD}, \mathbf{U}_{RD})\}, \\ S_U|_\Lambda &= \max\{S_R(\mathbf{U}_{RD}, \mathbf{U}_{RU}), S_R(\mathbf{U}_{LD}, \mathbf{U}_{LU})\}, \\ S_D|_\Lambda &= \min\{S_L(\mathbf{U}_{RD}, \mathbf{U}_{RU}), S_R(\mathbf{U}_{LD}, \mathbf{U}_{LU})\} \end{aligned}$$

to match the wave speeds of the nodal DG scheme in the cell. Denote

$$\mathcal{S}_R = \max\{S_R, 0\}, \quad \mathcal{S}_U = \max\{S_U, 0\}, \quad \mathcal{S}_L = \min\{S_L, 0\}, \quad \mathcal{S}_D = \min\{S_D, 0\},$$

then the value of  $\tilde{E}_z$  is given by

$$\begin{aligned} \tilde{E}_z^{HLL} &= \frac{1}{4} (E_z^{*,R} + E_z^{*,L} + E_z^{*,U} + E_z^{*,D}) \\ &\quad - \frac{1}{4} \mathcal{S}_U (B_x^{U,*} - B_x^{**}) - \frac{1}{4} \mathcal{S}_D (B_x^{D,*} - B_x^{**}) \\ &\quad + \frac{1}{4} \mathcal{S}_R (B_y^{R,*} - B_y^{**}) + \frac{1}{4} \mathcal{S}_L (B_y^{L,*} - B_y^{**}), \end{aligned}$$

where

$$\begin{aligned} E_z^{*,R} &= \hat{\mathbf{G}}_6^{HLL}(\mathbf{U}_{RD}, \mathbf{U}_{RU}), \quad E_z^{*,L} = \hat{\mathbf{G}}_6^{HLL}(\mathbf{U}_{LD}, \mathbf{U}_{LU}), \\ E_z^{*,U} &= -\hat{\mathbf{F}}_7^{HLL}(\mathbf{U}_{LU}, \mathbf{U}_{RU}), \quad E_z^{*,D} = -\hat{\mathbf{F}}_7^{HLL}(\mathbf{U}_{LD}, \mathbf{U}_{RD}), \end{aligned}$$

and

$$\begin{aligned} B_x^{**} &= \frac{1}{2\Delta\mathcal{S}} [2\mathcal{S}_R\mathcal{S}_U B_x^{RU} - 2\mathcal{S}_L\mathcal{S}_U B_x^{LU} - 2\mathcal{S}_R\mathcal{S}_D B_x^{RD} + 2\mathcal{S}_L\mathcal{S}_D B_x^{LD} \\ &\quad - \mathcal{S}_R (E_z^{RU} - E_z^{RD}) + \mathcal{S}_L (E_z^{LU} - E_z^{LD}) \\ &\quad - (\mathcal{S}_R - \mathcal{S}_L) (E_z^{*,U} - E_z^{*,D})], \end{aligned}$$

$$\begin{aligned}
B_y^{**} = & \frac{1}{2\Delta\mathcal{S}} [2\mathcal{S}_R\mathcal{S}_U B_y^{RU} - 2\mathcal{S}_L\mathcal{S}_U B_y^{LU} - 2\mathcal{S}_R\mathcal{S}_D B_y^{RD} + 2\mathcal{S}_L\mathcal{S}_D B_y^{LD} \\
& + \mathcal{S}_U (E_z^{RU} - E_z^{LU}) - \mathcal{S}_D (E_z^{RD} - E_z^{LD}) \\
& + (\mathcal{S}_U - \mathcal{S}_D) (E_z^{*,R} - E_z^{*,L})],
\end{aligned}$$

where  $\Delta\mathcal{S} = (\mathcal{S}_R - \mathcal{S}_L)(\mathcal{S}_U - \mathcal{S}_D)$ .

### Appendix C. Proof of Theorem 3.6.

*Proof.* Firstly, we prove the local entropy conservative (3.6). In each cell  $K_{i,j}$ , with the help of the semi-discrete nodal DG scheme (3.1) we have that

$$\begin{aligned}
\frac{d}{dt} \left( \frac{\Delta x \Delta y}{4} \sum_{i_1, j_1=0}^{k+1} \omega_{i_1} \omega_{j_1} \mathcal{U}_{i_1, j_1}^{i, j} \right) &= \frac{\Delta x \Delta y}{4} \sum_{i_1, j_1=0}^{k+1} \omega_{i_1} \omega_{j_1} \left( \mathbf{V}_{i_1, j_1}^{i, j} \right)^T \frac{d\mathbf{U}_{i_1, j_1}^{i, j}}{dt} \\
&= -\frac{\Delta y}{2} \sum_{j_1=0}^{k+1} \omega_{j_1} \sum_{i_1, l=0}^{k+1} 2S_{i_1, l} \left( \mathbf{V}_{i_1, j_1}^{i, j} \right)^T \mathbf{F}^S \left( \mathbf{U}_{i_1, j_1}^{i, j}, \mathbf{U}_{l, j_1}^{i, j} \right) \\
&\quad + \frac{\Delta y}{2} \sum_{j_1=0}^{k+1} \omega_{j_1} \sum_{i_1=0}^{k+1} \tau_{i_1} \left( \left( \mathbf{V}_{i_1, j_1}^{i, j} \right)^T \mathbf{F}_{i_1, j_1}^{i, j} - \left( \mathbf{V}_{i_1, j_1}^{i, j} \right)^T \mathbf{F}_{i_1, j_1}^{*, i, j} \right) \\
&\quad - \frac{\Delta x}{2} \sum_{i_1=0}^{k+1} \omega_{i_1} \sum_{j_1, l=0}^{k+1} 2S_{j_1, l} \left( \mathbf{V}_{i_1, j_1}^{i, j} \right)^T \mathbf{G}^S \left( \mathbf{U}_{i_1, j_1}^{i, j}, \mathbf{U}_{i_1, l}^{i, j} \right) \\
&\quad + \frac{\Delta x}{2} \sum_{i_1=0}^{k+1} \omega_{i_1} \sum_{j_1=0}^{k+1} \tau_{j_1} \left( \left( \mathbf{V}_{i_1, j_1}^{i, j} \right)^T \mathbf{G}_{i_1, j_1}^{i, j} - \left( \mathbf{V}_{i_1, j_1}^{i, j} \right)^T \mathbf{G}_{i_1, j_1}^{*, i, j} \right) \\
&=: T_1 + T_2 + T_3 + T_4.
\end{aligned}$$

For  $T_1$ , utilizing the SBP property yields

$$\begin{aligned}
-\frac{2}{\Delta y} T_1 &= \sum_{j_1=0}^{k+1} \omega_{j_1} \sum_{i_1, l=0}^{k+1} (S_{i_1, l} + B_{i_1, l} - S_{l, i_1}) \left( \mathbf{V}_{i_1, j_1}^{i, j} \right)^T \mathbf{F}^S \left( \mathbf{U}_{i_1, j_1}^{i, j}, \mathbf{U}_{l, j_1}^{i, j} \right) \\
&= \sum_{j_1=0}^{k+1} \omega_{j_1} \sum_{i_1=0}^{k+1} \tau_{i_1} \left( \mathbf{V}_{i_1, j_1}^{i, j} \right)^T \mathbf{F}_{i_1, j_1}^{i, j} \\
&\quad + \sum_{j_1=0}^{k+1} \omega_{j_1} \sum_{i_1, l=0}^{k+1} (S_{i_1, l} - S_{l, i_1}) \left( \mathbf{V}_{i_1, j_1}^{i, j} \right)^T \mathbf{F}^S \left( \mathbf{U}_{i_1, j_1}^{i, j}, \mathbf{U}_{l, j_1}^{i, j} \right).
\end{aligned}$$

According to the definition of entropy conservative flux (3.2), we get

$$\begin{aligned}
&\sum_{j_1=0}^{k+1} \omega_{j_1} \sum_{i_1, l=0}^{k+1} (S_{i_1, l} - S_{l, i_1}) \left( \mathbf{V}_{i_1, j_1}^{i, j} \right)^T \mathbf{F}^S \left( \mathbf{U}_{i_1, j_1}^{i, j}, \mathbf{U}_{l, j_1}^{i, j} \right) \\
&= \sum_{j_1=0}^{k+1} \omega_{j_1} \sum_{i_1, l=0}^{k+1} S_{i_1, l} \left( \mathbf{V}_{i_1, j_1}^{i, j} - \mathbf{V}_{l, j_1}^{i, j} \right)^T \mathbf{F}^S \left( \mathbf{U}_{i_1, j_1}^{i, j}, \mathbf{U}_{l, j_1}^{i, j} \right) \\
&= \sum_{j_1=0}^{k+1} \omega_{j_1} \sum_{i_1, l=0}^{k+1} S_{i_1, l} \left( \psi_{F, i_1, j_1}^{i, j} - \psi_{F, l, j_1}^{i, j} \right)
\end{aligned}$$



$$-\sum_{j_1=0}^{k+1} \omega_{j_1} \sum_{i_1, l=0}^{k+1} S_{i_1, l} \left( \phi_{i_1, j_1}^{i, j} - \phi_{l, j_1}^{i, j} \right) \frac{B_{x, i_1, j_1}^{i, j} + B_{x, l, j_1}^{i, j}}{2}.$$

For the first term, we have

$$\sum_{j_1=0}^{k+1} \omega_{j_1} \sum_{i_1, l=0}^{k+1} S_{i_1, l} \left( \psi_{F, i_1, j_1}^{i, j} - \psi_{F, l, j_1}^{i, j} \right) = - \sum_{j_1=0}^{k+1} \omega_{j_1} \sum_{i_1=0}^{k+1} \tau_{i_1} \psi_{F, i_1, j_1}^{i, j}.$$

For the second term, we have

$$\begin{aligned} & \sum_{j_1=0}^{k+1} \omega_{j_1} \sum_{i_1, l=0}^{k+1} S_{i_1, l} \left( \phi_{i_1, j_1}^{i, j} - \phi_{l, j_1}^{i, j} \right) \frac{B_{x, i_1, j_1}^{i, j} + B_{x, l, j_1}^{i, j}}{2} \\ &= \frac{1}{2} \sum_{j_1=0}^{k+1} \omega_{j_1} \sum_{i_1, l=0}^{k+1} S_{i_1, l} \left[ \left( \phi_{i_1, j_1}^{i, j} B_{x, i_1, j_1}^{i, j} - \phi_{l, j_1}^{i, j} B_{x, l, j_1}^{i, j} \right) + \left( \phi_{i_1, j_1}^{i, j} B_{x, l, j_1}^{i, j} - \phi_{l, j_1}^{i, j} B_{x, i_1, j_1}^{i, j} \right) \right] \\ &= \frac{1}{2} \sum_{j_1=0}^{k+1} \omega_{j_1} \sum_{i_1=0}^{k+1} \phi_{i_1, j_1}^{i, j} B_{x, i_1, j_1}^{i, j} \sum_{l=0}^{k+1} S_{i_1, l} - \frac{1}{2} \sum_{j_1=0}^{k+1} \omega_{j_1} \sum_{l=0}^{k+1} \phi_{l, j_1}^{i, j} B_{x, l, j_1}^{i, j} \sum_{i_1=0}^{k+1} S_{i_1, l} \\ &\quad + \frac{1}{2} \sum_{j_1=0}^{k+1} \omega_{j_1} \sum_{i_1, l=0}^{k+1} \phi_{i_1, j_1}^{i, j} B_{x, l, j_1}^{i, j} (S_{i_1, l} - S_{l, i_1}) \\ &= \sum_{j_1=0}^{k+1} \omega_{j_1} \sum_{i_1, l=0}^{k+1} \phi_{i_1, j_1}^{i, j} B_{x, l, j_1}^{i, j} S_{i_1, l} - \sum_{j_1=0}^{k+1} \omega_{j_1} \sum_{i_1=0}^{k+1} \tau_{i_1} \phi_{i_1, j_1}^{i, j} B_{x, i_1, j_1}^{i, j}. \end{aligned}$$

By the divergence-free property (3.5),

$$\begin{aligned} -\frac{2}{\Delta y} T_1 &= \sum_{j_1=0}^{k+1} \omega_{j_1} \sum_{i_1=0}^{k+1} \tau_{i_1} \left( \mathbf{v}_{i_1, j_1}^{i, j} \right)^T \mathbf{F}_{i_1, j_1}^{i, j} - \sum_{j_1=0}^{k+1} \omega_{j_1} \sum_{i_1=0}^{k+1} \tau_{i_1} \psi_{F, i_1, j_1}^{i, j} \\ &= \sum_{j_1=0}^{k+1} \omega_{j_1} \left( \left( \mathbf{v}_{k+1, j_1}^{i, j} \right)^T \mathbf{F}_{k+1, j_1}^{i, j} - \left( \mathbf{v}_{0, j_1}^{i, j} \right)^T \mathbf{F}_{0, j_1}^{i, j} \right) - \sum_{j_1=0}^{k+1} \omega_{j_1} (\psi_{F, k+1, j_1}^{i, j} - \psi_{F, 0, j_1}^{i, j}) \\ &\quad - \sum_{j_1=0}^{k+1} \omega_{j_1} \sum_{i_1, l=0}^{k+1} \phi_{i_1, j_1}^{i, j} B_{x, l, j_1}^{i, j} S_{i_1, l} + \sum_{j_1=0}^{k+1} \omega_{j_1} (\phi_{k+1, j_1}^{i, j} B_{x, j_1}^{i+1/2, j} - \phi_{0, j_1}^{i, j} B_{x, j_1}^{i-1/2, j}). \end{aligned}$$

Hence,

$$T_1 + T_2 = -\frac{\Delta y}{2} \sum_{j_1=0}^{k+1} \omega_{j_1} \left( \mathcal{F}_{k+1, j_1}^{*, i, j} - \mathcal{F}_{0, j_1}^{*, i, j} \right) + \frac{\Delta y}{2} \sum_{j_1=0}^{k+1} \omega_{j_1} \sum_{i_1, l=0}^{k+1} \phi_{i_1, j_1}^{i, j} B_{x, l, j_1}^{i, j} S_{i_1, l}.$$

Similarly,

$$T_3 + T_4 = -\frac{\Delta x}{2} \sum_{i_1=0}^{k+1} \omega_{i_1} \left( \mathcal{G}_{i_1, k+1}^{*, i, j} - \mathcal{G}_{i_1, 0}^{*, i, j} \right) + \frac{\Delta x}{2} \sum_{i_1=0}^{k+1} \omega_{i_1} \sum_{j_1, l=0}^{k+1} \phi_{i_1, j_1}^{i, j} B_{y, i_1, l}^{i, j} S_{j_1, l}.$$

Again, using the divergence-free property (3.4) yields

$$\begin{aligned} & \frac{\Delta y}{2} \sum_{j_1=0}^{k+1} \omega_{j_1} \sum_{i_1, l=0}^{k+1} \phi_{i_1, j_1}^{i, j} B_{x, l, j_1}^{i, j} S_{i_1, l} + \frac{\Delta x}{2} \sum_{i_1=0}^{k+1} \omega_{i_1} \sum_{j_1, l=0}^{k+1} \phi_{i_1, j_1}^{i, j} B_{y, i_1, l}^{i, j} S_{j_1, l} \\ &= \frac{\Delta x \Delta y}{4} \sum_{i_1, j_1=0}^{k+1} \omega_{i_1} \omega_{j_1} \phi_{i_1, j_1}^{i, j} \sum_{l=0}^{k+1} \left( \frac{2}{\Delta x} D_{i_1, l} B_{x, l, j_1}^{i, j} + \frac{2}{\Delta y} D_{j_1, l} B_{y, i_1, l}^{i, j} \right) = 0. \end{aligned}$$

Therefore,

$$\begin{aligned} \text{(C.1)} \quad & \frac{d}{dt} \left( \frac{\Delta x \Delta y}{4} \sum_{i_1, j_1=0}^{k+1} \omega_{i_1} \omega_{j_1} \mathcal{U}_{i_1, j_1}^{i, j} \right) = T_1 + T_2 + T_3 + T_4 \\ &= -\frac{\Delta y}{2} \sum_{j_1=0}^{k+1} \omega_{j_1} \left( \mathcal{F}_{k+1, j_1}^{*, i, j} - \mathcal{F}_{0, j_1}^{*, i, j} \right) - \frac{\Delta x}{2} \sum_{i_1=0}^{k+1} \omega_{i_1} \left( \mathcal{G}_{i_1, k+1}^{*, i, j} - \mathcal{G}_{i_1, 0}^{*, i, j} \right). \end{aligned}$$

Next, we prove the global entropy stable. At interface  $I_{i+1/2, j}^y$  inside the computational domain  $\Omega$ , by using the definition of entropy stable flux, we can obtain

$$\begin{aligned} \text{(C.2)} \quad & - \left( \mathcal{F}_{k+1, j_1}^{*, i, j} - \mathcal{F}_{0, j_1}^{*, i+1, j} \right) \\ &= \left( \mathbf{V}_{0, j_1}^{i+1, j} - \mathbf{V}_{k+1, j_1}^{i, j} \right)^T \hat{\mathbf{F}}_{j_1}^{i+1/2, j} - \left( \psi_{F, 0, j_1}^{i+1, j} - \psi_{F, k+1, j_1}^{i, j} \right) \\ &\quad + \frac{B_{x, 0, j_1}^{i+1, j} + B_{x, k+1, j_1}^{i, j}}{2} \left( \phi_{0, j_1}^{i+1, j} - \phi_{k+1, j_1}^{i, j} \right) \\ &\leq 0. \end{aligned}$$

If the boundaries are periodic or compactly supported, then (C.2) also hold for the boundaries of  $\Omega$ . Similarly,  $-\left( \mathcal{G}_{i_1, k+1}^{*, i, j} - \mathcal{G}_{i_1, 0}^{*, i, j+1} \right) \leq 0$ . Furthermore, summing (C.1) over  $i, j$  yields

$$\frac{d}{dt} \left( \frac{\Delta x \Delta y}{4} \sum_{i, j=1}^{N_x, N_y} \sum_{i_1, j_1=0}^{k+1} \omega_{i_1} \omega_{j_1} \mathcal{U}_{i_1, j_1}^{i, j} \right) \leq 0.$$

For reflective walls, without loss of generality, we assume the left boundary  $x_{1/2} = a$  is a reflective wall, i.e.

$$\mathbf{U}_{int} = (\rho, u_x, u_y, u_z, \mathcal{E}, B_x, B_y, B_z)^T, \quad \mathbf{U}_{out} = (\rho, -u_x, u_y, u_z, \mathcal{E}, -B_x, B_y, B_z)^T.$$

We can verify that  $S_R = -S_L =: S$ , thus the HLL flux is equivalent to the Lax-Friedrichs flux. Notice that the condition (3.5) leads to  $B_x = 0$ , hence

$$\begin{aligned} \hat{\mathbf{F}}(\mathbf{U}_{out}, \mathbf{U}_{int}) &= \frac{1}{2} [\mathbf{F}(\mathbf{U}_{out}) + \mathbf{F}(\mathbf{U}_{int})] - \frac{S}{2} (\mathbf{U}_{int} - \mathbf{U}_{out}) \\ &= [0, p^* - \rho u_x S, 0, 0, 0, 0, 0, 0]^T, \end{aligned}$$

and

$$\mathbf{V}_{int} - \mathbf{V}_{out} = 4\beta u_x, \quad \psi_{int} - \psi_{out} = 2\rho u_x + 2\beta u_x \|\mathbf{B}\|^2.$$

Then, it can be calculated that

$$\begin{aligned}
 -(\mathcal{F}^{*,int} - \mathcal{F}^{*,out}) &= (\mathbf{V}_{int} - \mathbf{V}_{out})^T \hat{\mathbf{F}}(\mathbf{U}_{out}, \mathbf{U}_{int}) - (\psi_{int} - \psi_{out}) \\
 &= 4\frac{\rho}{2p}u_x \left( p + \frac{1}{2} \|\mathbf{B}\|^2 - \rho u_x S \right) - 2\rho u_x + 2\frac{\rho}{2p}u_x \|\mathbf{B}\|^2 \\
 &= -4\beta\rho u_x^2 S \leq 0,
 \end{aligned}$$

i.e. the entropy dissipate property (C.2) also holds for reflective walls. And the entropy dissipate on the whole domain holds as well.  $\square$

#### Appendix D. The reconstruction for small $k$ .

We give a brief discussion about the LS reconstruction problem in Section 3.3 for small  $k$ . We rewrite the linear system (3.18) as

$$\mathbf{G} \begin{bmatrix} \mathbf{B}^{rec} \\ \boldsymbol{\lambda} \end{bmatrix} = \begin{bmatrix} M_2 \tilde{\mathbf{B}} \\ \mathbf{b}_1 \end{bmatrix},$$

then  $\mathbf{G}^{-1}$  can be given by

$$\mathbf{G}^{-1} = \begin{bmatrix} M^{-1} - M^{-1}A_1^T \mathbf{S} A_1 M^{-1} & M^{-1}A_1^T \mathbf{S} \\ -\mathbf{S} A_1 M^{-1} & \mathbf{S} \end{bmatrix},$$

where  $\mathbf{S} = (A_1 M A_1^T)^{-1}$  is the Schur complement of  $M$ . In the following, we will assume  $\Delta x = \Delta y$ .

To help understand, we first consider the simplest case  $k = 0$ , and the 2 points Gauss-Lobatto quadrature is used. Now we have

$$M = \begin{bmatrix} 1 & 0 \\ 0 & 1 \end{bmatrix} = I, \quad D = \begin{bmatrix} 0.5 & -0.5 \\ 0.5 & -0.5 \end{bmatrix}.$$

Assume

$$b_x^+ = a_0^+, \quad b_x^- = a_0^-, \quad b_y^+ = b_0^+, \quad b_y^- = b_0^-.$$

Then, the original linear system of reconstruction (3.16) is

$$(D.1) \quad \begin{bmatrix} -1 & 1 & 0 & 0 & -1 & 0 & 1 & 0 \\ -1 & 1 & 0 & 0 & 0 & -1 & 0 & 1 \\ 0 & 0 & -1 & 1 & -1 & 0 & 1 & 0 \\ 0 & 0 & -1 & 1 & 0 & -1 & 0 & 1 \\ 0 & 1 & 0 & 0 & 0 & 0 & 0 & 0 \\ 0 & 0 & 0 & 1 & 0 & 0 & 0 & 0 \\ 1 & 0 & 0 & 0 & 0 & 0 & 0 & 0 \\ 0 & 0 & 1 & 0 & 0 & 0 & 0 & 0 \\ 0 & 0 & 0 & 0 & 0 & 0 & 1 & 0 \\ 0 & 0 & 0 & 0 & 0 & 0 & 0 & 1 \\ 0 & 0 & 0 & 0 & 1 & 0 & 0 & 0 \\ 0 & 0 & 0 & 0 & 0 & 1 & 0 & 0 \end{bmatrix} \begin{bmatrix} B_{x,00} \\ B_{x,10} \\ B_{x,01} \\ B_{x,11} \\ B_{y,00} \\ B_{y,10} \\ B_{y,01} \\ B_{y,11} \end{bmatrix} = \begin{bmatrix} 0 \\ 0 \\ 0 \\ 0 \\ a_0^+ \\ a_0^+ \\ a_0^- \\ a_0^- \\ b_0^+ \\ b_0^+ \\ b_0^- \\ b_0^- \end{bmatrix},$$

which is a  $12 \times 8$  linear system. To simplify the form, we have multiplied a factor 2 for the first four rows. It is notable that the last 8 rows of  $A$  already form a full rank  $8 \times 8$  matrix, hence the system (D.1) has at most one solution. Since the number of equations is larger than DOFs, it seems that there may have “ $0 = d$ ” rows with

$d \neq 0$  in the simplified stepped system, which will lead to the system non-solvable. However, applying some elementary row operations to  $A$  yields

$$\begin{bmatrix} 0 & 0 & 0 & 0 & 0 & 0 & 0 & 0 \\ 0 & 0 & 0 & 0 & 0 & 0 & 0 & 0 \\ 0 & 0 & 0 & 0 & 0 & 0 & 0 & 0 \\ 0 & 0 & 0 & 0 & 0 & 0 & 0 & 0 \\ 0 & 1 & 0 & 0 & 0 & 0 & 0 & 0 \\ 0 & 0 & 0 & 1 & 0 & 0 & 0 & 0 \\ 1 & 0 & 0 & 0 & 0 & 0 & 0 & 0 \\ 0 & 0 & 1 & 0 & 0 & 0 & 0 & 0 \\ 0 & 0 & 0 & 0 & 0 & 0 & 1 & 0 \\ 0 & 0 & 0 & 0 & 0 & 0 & 0 & 1 \\ 0 & 0 & 0 & 0 & 1 & 0 & 0 & 0 \\ 0 & 0 & 0 & 0 & 0 & 1 & 0 & 0 \end{bmatrix} \begin{bmatrix} B_{x,00} \\ B_{x,10} \\ B_{x,01} \\ B_{x,11} \\ B_{y,00} \\ B_{y,10} \\ B_{y,01} \\ B_{y,11} \end{bmatrix} = \begin{bmatrix} a_0^- - a_0^+ + b_0^- - b_0^+ \\ a_0^- - a_0^+ + b_0^- - b_0^+ \\ a_0^- - a_0^+ + b_0^- - b_0^+ \\ a_0^- - a_0^+ + b_0^- - b_0^+ \\ a_0^+ \\ a_0^+ \\ a_0^- \\ a_0^- \\ b_0^+ \\ b_0^+ \\ b_0^- \\ b_0^- \end{bmatrix}.$$

Hence, the system is solvable if and only if the cell-average constraint is satisfied, which indicates that

$$a_0^+ - a_0^- + b_0^+ - b_0^- = 0.$$

Then, the unique solution of (D.1) is

$$(D.2) \quad \begin{aligned} B_{x,00} = B_{x,01} = a_0^-, \quad B_{x,10} = B_{x,11} = a_0^+, \\ B_{y,00} = B_{y,10} = b_0^-, \quad B_{y,01} = B_{y,11} = b_0^+. \end{aligned}$$

On the other hand, if we directly consider the system (3.18), then we can see  $A_1$  is a  $8 \times 8$  full rank matrix. Since  $M = I$ , we can derive that  $\mathbf{S} = (A_1^T)^{-1} A_1^{-1}$ , and

$$\mathbf{G}^{-1} = \begin{bmatrix} O & A_1^{-1} \\ -(A_1^T)^{-1} & (A_1^T)^{-1} A_1^{-1} \end{bmatrix}.$$

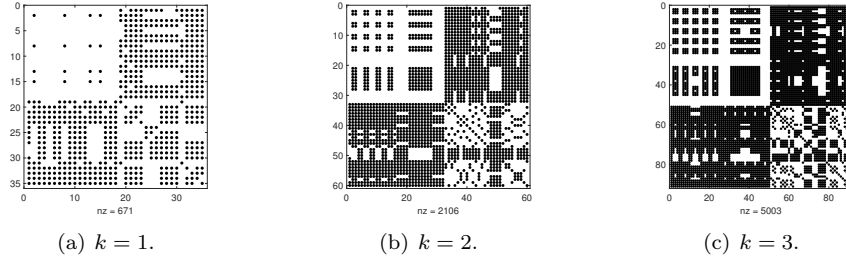
Therefore, we have

$$\begin{bmatrix} \mathbf{B}^{rec} \\ \lambda \end{bmatrix} = \begin{bmatrix} O & A_1^{-1} \\ -(A_1^T)^{-1} & (A_1^T)^{-1} A_1^{-1} \end{bmatrix} \begin{bmatrix} \mathbf{B}^{DG} \\ \mathbf{b}_1 \end{bmatrix},$$

so  $\mathbf{B}^{rec} = A_1^{-1} \mathbf{b}_1$ , it is also the solution of  $\mathbf{A}\mathbf{B} = \mathbf{b}$ , thus we recover (D.2). This is also consistent with the conclusion in [5].

However, for  $k > 0$ , the system has become very complicated. When  $k = 1$ , the size of  $A$  is a  $21 \times 18$ , and the size of  $\mathbf{G}$  is  $35 \times 35$ . For  $k = 2$ , the sizes are respectively  $32 \times 32$  and  $60 \times 60$ . For  $k = 3$ , the sizes are respectively  $45 \times 50$  and  $91 \times 91$ . Therefore, it is difficult to study the underlying mechanism or give the explicit formulation like (D.2) for the reconstruction equation with general  $k$ . In Fig 15, we present the structure of nonzero elements in  $\mathbf{G}^{-1}$  for  $k = 1, 2, 3$  as a reference.

In addition, we give the full express of  $\mathbf{G}^{-1}$  for  $k = 1$ . The first 5 columns of  $\mathbf{G}^{-1}$  are


 FIG. 15. The structure of nonzero elements in  $\mathbf{G}^{-1}$ .

0	0	0	0	0
0	9/16	0	0	0
0	0	0	0	0
0	0	0	0	0
0	0	0	0	0
0	0	0	0	0
0	0	0	0	0
0	-9/16	0	0	0
0	0	0	0	0
0	0	0	0	0
0	0	0	0	0
0	0	0	0	0
0	-9/16	0	0	0
0	0	0	0	0
0	9/16	0	0	0
0	0	0	0	0
0	0	0	0	0
0	0	0	0	0
446/10487	-361/4426	446/10487	0	0
0	-407/5879	1345/18033	686/18395	-407/5879
194/2497	-811/8786	158/7263	2699/54280	-811/8786
-293/5856	482/5241	-293/5856	293/2928	-403/2191
31/13608	-236/56361	31/13608	-31/6804	225/26867
-195/1351	0	195/1351	-195/1351	0
1262/6927	0	-1262/6927	-1217/3340	0
5143/432011	0	-5143/432011	-10286/432011	0
-3599/5453	0	937/6487	-115/589	0
0	0	-137/1263	2539/11975	0
0	0	336/1285	609/3007	0
-99/90076	0	-1471/2543	513/7487	0
-338/963	-265/724	-338/963	0	0
152/7003	181/7664	152/7003	-304/7003	-181/3832
-883/3115	-223/723	-883/3115	847/1494	446/723
89/1024	884/2323	213/499	737/2869	884/2323
-413/985	-469/1397	-203/5977	-526/2321	-469/1397

Column 6 to 10 of  $\mathbf{G}^{-1}$  are

0	0	0	0	0
0	0	-9/16	0	0
0	0	0	0	0
0	0	0	0	0
0	0	0	0	0
0	0	0	0	0
0	0	0	0	0
0	0	9/16	0	0
0	0	0	0	0
0	0	0	0	0
0	0	0	0	0
0	0	0	0	0
0	0	9/16	0	0
0	0	0	0	0
0	0	-9/16	0	0
0	0	0	0	0
0	0	0	0	0
0	0	0	0	0
0	-446/10487	361/4426	-446/10487	446/10487
686/18395	1345/18033	-407/5879	0	-158/7263
2699/54280	158/7263	-811/8786	194/2497	1345/18033
293/2928	-293/5856	482/5241	-293/5856	-31/13608
-31/6804	31/13608	-236/56361	31/13608	-293/5856
195/1351	-195/1351	0	195/1351	-195/1351
1217/3340	1262/6927	0	-1262/6927	-5143/432011
10286/432011	5143/432011	0	-5143/432011	1262/6927
51/881	739/2742	0	-96/3349	491/831
723/6241	5078/11975	0	946/2781	-1395/8672
-162/1069	625/1543	0	-2033/3601	-341/1901
-809/2711	255/1846	0	-77/4190	524/3107
0	338/963	265/724	338/963	-338/963
-304/7003	152/7003	181/7664	152/7003	-883/3115
847/1494	-883/3115	-223/723	-883/3115	-152/7003
737/2869	213/499	884/2323	89/1024	-203/5977
-526/2321	-203/5977	-469/1397	-413/985	-213/499

Column 11 to 15 of  $\mathbf{G}^{-1}$  are

0	0	0	0	0
0	0	-9/16	0	9/16
0	0	0	0	0
0	0	0	0	0
0	0	0	0	0
0	0	0	0	0
0	0	0	0	0
0	0	9/16	0	-9/16
0	0	0	0	0
0	0	0	0	0
0	0	0	0	0
0	0	0	0	0
0	0	9/16	0	-9/16
0	0	0	0	0
0	0	-9/16	0	9/16
0	0	0	0	0
0	0	0	0	0
0	0	0	0	0
0	-446/10487	-361/4426	0	361/4426
-2699/54280	-194/2497	811/8786	811/8786	811/8786
686/18395	0	-407/5879	-407/5879	-407/5879
31/6804	-31/13608	236/56361	-225/26867	236/56361
293/2928	-293/5856	482/5241	-403/2191	482/5241
-195/1351	-195/1351	0	0	0
10286/432011	-5143/432011	0	0	0
-1217/3340	1262/6927	0	0	0
551/2084	-169/2723	0	0	0
-823/16086	301/5142	0	0	0
-3234/139709	461/3464	0	0	0
-572/2423	-1841/2873	0	0	0
0	338/963	-265/724	0	265/724
847/1494	-883/3115	-223/723	446/723	-223/723
304/7003	-152/7003	-181/7664	181/3832	-181/7664
-526/2321	-413/985	-469/1397	-469/1397	-469/1397
-737/2869	-89/1024	-884/2323	-884/2323	-884/2323

Column 16 to 20 of  $G^{-1}$  are

0	0	0	446/10487	0
0	0	0	-361/4426	-407/5879
0	0	0	446/10487	1345/18033
0	0	0	0	686/18395
0	0	0	0	-407/5879
0	0	0	0	686/18395
0	0	0	-446/10487	1345/18033
0	0	0	361/4426	-407/5879
0	0	0	-446/10487	0
0	0	0	446/10487	-158/7263
0	0	0	0	-2699/54280
0	0	0	-446/10487	-194/2497
0	0	0	-361/4426	811/8786
0	0	0	0	811/8786
0	0	0	361/4426	811/8786
0	0	0	446/10487	-194/2497
0	0	0	0	-2699/54280
0	0	0	-446/10487	-158/7263
446/10487	0	-446/10487	-23/1712	0
-194/2497	-2699/54280	-158/7263	0	-287/6896
0	686/18395	1345/18033	0	0
-31/13608	31/6804	-31/13608	0	-94/5141
-293/5856	293/2928	-293/5856	0	199/7414
195/1351	195/1351	195/1351	0	0
5143/432011	-10286/432011	5143/432011	0	0
-1262/6927	1217/3340	-1262/6927	0	0
1022/16221	31/2753	-251/6200	0	67/10675
357/604	401/8908	-731/1459	0	-27/6463
646/2335	961/2904	3219/8357	0	63/14102
222/2929	120/917	3951/21250	0	56/50269
-338/963	0	338/963	-90/2261	0
-883/3115	847/1494	-883/3115	0	-65/1076
-152/7003	304/7003	-152/7003	0	144/3743
-413/985	-526/2321	-203/5977	0	199/1660
-89/1024	-737/2869	-213/499	0	62/2495



The 21 to 25 columns of  $\mathbf{G}^{-1}$  are

0	0	0	446/10487	0
0	0	0	-361/4426	-407/5879
0	0	0	446/10487	1345/18033
0	0	0	0	686/18395
0	0	0	0	-407/5879
0	0	0	0	686/18395
0	0	0	-446/10487	1345/18033
0	0	0	361/4426	-407/5879
0	0	0	-446/10487	0
0	0	0	446/10487	-158/7263
0	0	0	0	-2699/54280
0	0	0	-446/10487	-194/2497
0	0	0	-361/4426	811/8786
0	0	0	0	811/8786
0	0	0	361/4426	811/8786
0	0	0	446/10487	-194/2497
0	0	0	0	-2699/54280
0	0	0	-446/10487	-158/7263
446/10487	0	-446/10487	-23/1712	0
-194/2497	-2699/54280	-158/7263	0	-287/6896
0	686/18395	1345/18033	0	0
-31/13608	31/6804	-31/13608	0	-94/5141
-293/5856	293/2928	-293/5856	0	199/7414
195/1351	195/1351	195/1351	0	0
5143/432011	-10286/432011	5143/432011	0	0
-1262/6927	1217/3340	-1262/6927	0	0
1022/16221	31/2753	-251/6200	0	67/10675
357/604	401/8908	-731/1459	0	-27/6463
646/2335	961/2904	3219/8357	0	63/14102
222/2929	120/917	3951/21250	0	56/50269
-338/963	0	338/963	-90/2261	0
-883/3115	847/1494	-883/3115	0	-65/1076
-152/7003	304/7003	-152/7003	0	144/3743
-413/985	-526/2321	-203/5977	0	199/1660
-89/1024	-737/2869	-213/499	0	62/2495

Column 26 to 30 of  $\mathbf{G}^{-1}$  are

5143/432011	-3599/5453	0	0	-99/90076
0	0	0	0	0
-5143/432011	937/6487	-137/1263	336/1285	-1471/2543
-10286/432011	-115/589	2539/11975	609/3007	513/7487
0	0	0	0	0
10286/432011	51/881	723/6241	-162/1069	-809/2711
5143/432011	739/2742	5078/11975	625/1543	255/1846
0	0	0	0	0
-5143/432011	-96/3349	946/2781	-2033/3601	-77/4190
1262/6927	491/831	-1395/8672	-341/1901	524/3107
-1217/3340	551/2084	-823/16086	-3234/139709	-572/2423
1262/6927	-169/2723	301/5142	461/3464	-1841/2873
0	0	0	0	0
0	0	0	0	0
0	0	0	0	0
-1262/6927	1022/16221	357/604	646/2335	222/2929
1217/3340	31/2753	401/8908	961/2904	120/917
-1262/6927	-251/6200	-731/1459	3219/8357	3951/21250
0	0	0	0	0
0	67/10675	-27/6463	63/14102	56/50269
0	-74/64347	-111/20717	-45/9634	95/18561
0	53/12731	-68/6223	-45/20756	152/19417
0	-90/9571	21/29873	-61/5987	37/11708
-149/3989	0	0	0	0
0	-49/1496	110/8839	81/1768	145/3054
-2/15	429/14929	-61/5587	-91/2264	-142/3409
429/14929	-797/5375	107/6728	56/3313	182/5961
-61/5587	107/6728	-297/2248	-112/8103	8/11573
-91/2264	56/3313	-112/8103	-425/2513	-175/4867
-142/3409	182/5961	8/11573	-175/4867	-1250/7501
0	0	0	0	0
0	-332/6139	59/9990	-285/4963	92/5557
0	131/5963	-80/1293	-155/11002	277/6160
0	106/3253	-178/6237	87/4607	179/15250
0	632/47779	239/9859	216/7151	-429/16265

Column 31 to 35 of  $\mathbf{G}^{-1}$  are

-338/963	152/7003	-883/3115	89/1024	-413/985
-265/724	181/7664	-223/723	884/2323	-469/1397
-338/963	152/7003	-883/3115	213/499	-203/5977
0	-304/7003	847/1494	737/2869	-526/2321
0	-181/3832	446/723	884/2323	-469/1397
0	-304/7003	847/1494	737/2869	-526/2321
338/963	152/7003	-883/3115	213/499	-203/5977
265/724	181/7664	-223/723	884/2323	-469/1397
338/963	152/7003	-883/3115	89/1024	-413/985
-338/963	-883/3115	-152/7003	-203/5977	-213/499
0	847/1494	304/7003	-526/2321	-737/2869
338/963	-883/3115	-152/7003	-413/985	-89/1024
-265/724	-223/723	-181/7664	-469/1397	-884/2323
0	446/723	181/3832	-469/1397	-884/2323
265/724	-223/723	-181/7664	-469/1397	-884/2323
-338/963	-883/3115	-152/7003	-413/985	-89/1024
0	847/1494	304/7003	-526/2321	-737/2869
338/963	-883/3115	-152/7003	-203/5977	-213/499
-90/2261	0	0	0	0
0	-65/1076	144/3743	199/1660	62/2495
0	144/3743	65/1076	62/2495	-199/1660
0	-17/3218	573/3355	298/4075	-217/3070
0	573/3355	17/3218	-217/3070	-298/4075
0	0	0	0	0
0	0	0	0	0
0	0	0	0	0
0	-332/6139	131/5963	106/3253	632/47779
0	59/9990	-80/1293	-178/6237	239/9859
0	-285/4963	-155/11002	87/4607	216/7151
0	92/5557	277/6160	179/15250	-429/16265
-202/581	0	0	0	0
0	-1189/1092	0	473/1203	356/931
0	0	-1189/1092	-356/931	473/1203
0	473/1203	-356/931	-1321/1514	0
0	356/931	473/1203	0	-1321/1514

## REFERENCES

- [1] M. ABD EL-NABY, E. M. ELBARBARY, AND N. Y. ABDELAZEM, *Finite difference solution of radiation effects on MHD unsteady free-convection flow over vertical plate with variable surface temperature*, (2003).
- [2] R. ABGRALL, *A general framework to construct schemes satisfying additional conservation relations. Application to entropy conservative and entropy dissipative schemes*, Journal of Computational Physics, (2018).
- [3] D. S. BALSARA, *Second-order-accurate schemes for magnetohydrodynamics with divergence-free reconstruction*, The Astrophysical Journal Supplement Series, 151 (2004), p. 149.
- [4] D. S. BALSARA AND J. KIM, *A comparison between divergence-cleaning and staggered-mesh formulations for numerical magnetohydrodynamics*, The Astrophysical Journal, 602 (2004), p. 1079.
- [5] D. S. BALSARA, R. KUMAR, AND P. CHANDRASHEKAR, *Globally divergence-free DG scheme for ideal compressible MHD*, Communications in Applied Mathematics and Computational

- Science, 16 (2021), pp. 59–98.
- [6] D. S. BALSARA AND D. S. SPICER, *A staggered mesh algorithm using high order Godunov fluxes to ensure solenoidal magnetic fields in magnetohydrodynamic simulations*, Journal of Computational Physics, 149 (1999), pp. 270–292.
  - [7] F. BOUCHUT, C. KLINGENBERG, AND K. WAAGAN, *A multiwave approximate Riemann solver for ideal MHD based on relaxation. I: theoretical framework*, Numerische Mathematik, 108 (2007), pp. 7–42.
  - [8] F. BOUCHUT, C. KLINGENBERG, AND K. WAAGAN, *A multiwave approximate Riemann solver for ideal MHD based on relaxation II: numerical implementation with 3 and 5 waves*, Numerische Mathematik, 115 (2010), pp. 647–679.
  - [9] F. BREZZI, J. DOUGLAS, AND L. D. MARINI, *Two families of mixed finite elements for second order elliptic problems*, Numerische Mathematik, 47 (1985), pp. 217–235.
  - [10] M. BRIO AND C. C. WU, *An upwind differencing scheme for the equations of ideal magnetohydrodynamics*, Journal of computational physics, 75 (1988), pp. 400–422.
  - [11] J. CHAN, *On discretely entropy conservative and entropy stable discontinuous Galerkin methods*, Journal of Computational Physics, 362 (2018), pp. 346–374.
  - [12] J. CHAN, *Skew-symmetric entropy stable modal discontinuous Galerkin formulations*, Journal of Scientific Computing, 81 (2019), pp. 459–485.
  - [13] P. CHANDRASHEKAR AND C. KLINGENBERG, *Entropy stable finite volume scheme for ideal compressible MHD on 2-D Cartesian meshes*, SIAM Journal on Numerical Analysis, 54 (2016), pp. 1313–1340.
  - [14] P. CHANDRASHEKAR AND R. KUMAR, *Constraint preserving discontinuous Galerkin method for ideal compressible MHD on 2-D Cartesian grids*, Journal of Scientific Computing, 84 (2020), p. 39.
  - [15] T. CHEN AND C.-W. SHU, *Entropy stable high order discontinuous Galerkin methods with suitable quadrature rules for hyperbolic conservation laws*, Journal of Computational Physics, 345 (2017), pp. 427–461.
  - [16] A. J. CHRISTLIEB, X. FENG, Y. JIANG, AND Q. TANG, *A high-order finite difference WENO scheme for ideal magnetohydrodynamics on curvilinear meshes*, SIAM Journal on Scientific Computing, 40 (2018), pp. A2631–A2666.
  - [17] A. J. CHRISTLIEB, J. A. ROSSMANITH, AND Q. TANG, *Finite difference weighted essentially non-oscillatory schemes with constrained transport for ideal magnetohydrodynamics*, Journal of Computational Physics, 268 (2014), pp. 302–325.
  - [18] B. COCKBURN, S. HOU, AND C.-W. SHU, *The Runge-Kutta local projection discontinuous Galerkin finite element method for conservation laws. IV. The multidimensional case*, Mathematics of Computation, 54 (1990), pp. 545–581.
  - [19] B. COCKBURN, F. LI, AND C.-W. SHU, *Locally divergence-free discontinuous Galerkin methods for the Maxwell equations*, Journal of Computational Physics, 194 (2004), pp. 588–610.
  - [20] B. COCKBURN, S.-Y. LIN, AND C.-W. SHU, *TVB Runge-Kutta local projection discontinuous Galerkin finite element method for conservation laws III: one-dimensional systems*, Journal of computational Physics, 84 (1989), pp. 90–113.
  - [21] B. COCKBURN AND C.-W. SHU, *TVB Runge-Kutta local projection discontinuous Galerkin finite element method for conservation laws. II. General framework*, Mathematics of computation, 52 (1989), pp. 411–435.
  - [22] B. COCKBURN AND C.-W. SHU, *The Runge-Kutta local projection-discontinuous-Galerkin finite element method for scalar conservation laws*, ESAIM: Mathematical Modelling and Numerical Analysis, 25 (1991), pp. 337–361.
  - [23] B. COCKBURN AND C.-W. SHU, *The Runge-Kutta discontinuous Galerkin method for conservation laws V: multidimensional systems*, Journal of computational physics, 141 (1998), pp. 199–224.
  - [24] B. COCKBURN, C.-W. SHU, C. JOHNSON, E. TADMOR, AND C.-W. SHU, *Essentially non-oscillatory and weighted essentially non-oscillatory schemes for hyperbolic conservation laws*, Springer, 1998.
  - [25] A. DEDNER, F. KEMM, D. KRÖNER, C.-D. MUNZ, T. SCHNITZER, AND M. WESENBERG, *Hyperbolic divergence cleaning for the MHD equations*, Journal of Computational Physics, 175 (2002), pp. 645–673.
  - [26] C. R. EVANS AND J. F. HAWLEY, *Simulation of magnetohydrodynamic flows-A constrained transport method*, The Astrophysical Journal, 332 (1988), pp. 659–677.
  - [27] K. G. FELKER AND J. M. STONE, *A fourth-order accurate finite volume method for ideal MHD via upwind constrained transport*, Journal of Computational Physics, 375 (2018), pp. 1365–1400.
  - [28] U. S. FJORDHOLM, S. MISHRA, AND E. TADMOR, *Arbitrarily high-order accurate entropy stable*

- essentially nonoscillatory schemes for systems of conservation laws*, SIAM Journal on Numerical Analysis, 50 (2012), pp. 544–573.
- [29] P. FU, F. LI, AND Y. XU, *Globally divergence-free discontinuous Galerkin methods for ideal magnetohydrodynamic equations*, Journal of Scientific Computing, 77 (2018), pp. 1621–1659.
  - [30] E. GABURRO, P. ÖFFNER, M. RICCHIUTO, AND D. TORLO, *High order entropy preserving ADER-DG schemes*, Applied Mathematics and Computation, 440 (2023), p. 127644.
  - [31] T. A. GARDINER AND J. M. STONE, *An unsplit Godunov method for ideal MHD via constrained transport*, Journal of Computational Physics, 205 (2005), pp. 509–539.
  - [32] G. J. GASSNER, *A skew-symmetric discontinuous Galerkin spectral element discretization and its relation to SBP-SAT finite difference methods*, SIAM Journal on Scientific Computing, 35 (2013), pp. A1233–A1253.
  - [33] E. GODLEWSKI AND P. RAVIART, *Hyperbolic systems of conservation laws*, Ellipses Math, Appl, 1991.
  - [34] E. GODLEWSKI AND P.-A. RAVIART, *Numerical approximation of hyperbolic systems of conservation laws*, vol. 118, Springer Science & Business Media, 2013.
  - [35] S. GODUNOV, *Symmetric form of the equations of magnetohydrodynamics*, Numerical Methods for Mechanics of Continuum Medium, 1 (1972), pp. 26–34.
  - [36] K. HU, Y. MA, AND J. XU, *Stable finite element methods preserving  $\nabla \cdot \mathbf{B} = 0$  exactly for MHD models*, Numerische Mathematik, 135 (2017), pp. 371–396.
  - [37] T. JONES, J. B. GAALAAS, D. RYU, AND A. FRANK, *The MHD Kelvin-Helmholtz instability. II. The roles of weak and oblique fields in planar flows*, The Astrophysical Journal, 482 (1997), p. 230.
  - [38] D. I. KETCHESON, *Highly efficient strong stability-preserving Runge-Kutta methods with low-storage implementations*, SIAM Journal on Scientific Computing, 30 (2008), pp. 2113–2136.
  - [39] F. LI AND C.-W. SHU, *Locally divergence-free discontinuous Galerkin methods for MHD equations*, Journal of Scientific Computing, 22 (2005), pp. 413–442.
  - [40] F. LI, L. XU, AND S. YAKOVLEV, *Central discontinuous Galerkin methods for ideal MHD equations with the exactly divergence-free magnetic field*, Journal of Computational Physics, 230 (2011), pp. 4828–4847.
  - [41] Y. LIU, W. GUO, Y. JIANG, AND M. ZHANG, *Non-oscillatory entropy stable DG schemes for hyperbolic conservation law*, arXiv preprint arXiv:2410.16729, (2024).
  - [42] Y. LIU, C.-W. SHU, AND M. ZHANG, *Entropy stable high order discontinuous Galerkin methods for ideal compressible MHD on structured meshes*, Journal of Computational Physics, 354 (2018), pp. 163–178.
  - [43] J. LU, Y. LIU, AND C.-W. SHU, *An oscillation-free discontinuous Galerkin method for scalar hyperbolic conservation laws*, SIAM Journal on Numerical Analysis, 59 (2021), pp. 1299–1324.
  - [44] X.-H. LUO, B.-W. LI, J.-K. ZHANG, AND Z.-M. HU, *Simulation of thermal radiation effects on MHD free convection in a square cavity using the Chebyshev collocation spectral method*, Numerical Heat Transfer, Part A: Applications, 66 (2014), pp. 792–815.
  - [45] A. MALAGOLI, G. BODO, AND R. ROSNER, *On the nonlinear evolution of magnetohydrodynamic Kelvin-Helmholtz instabilities*, Astrophysical Journal v. 456, p. 708, 456 (1996), p. 708.
  - [46] A. MIGNONE, P. TZEFERACOS, AND G. BODO, *High-order conservative finite difference GLM-MHD schemes for cell-centered MHD*, Journal of Computational Physics, 229 (2010), pp. 5896–5920.
  - [47] T. MINOSHIMA, T. MIYOSHI, AND Y. MATSUMOTO, *A high-order weighted finite difference scheme with a multistate approximate Riemann solver for divergence-free magnetohydrodynamic simulations*, The Astrophysical Journal Supplement Series, 242 (2019), p. 14.
  - [48] M. PENG, Z. SUN, AND K. WU, *OEDG: Oscillation-eliminating discontinuous Galerkin method for hyperbolic conservation laws*, Mathematics of Computation, (2024).
  - [49] K. G. POWELL, P. L. ROE, T. J. LINDE, T. I. GOMBOSI, AND D. L. DE ZEEUW, *A solution-adaptive upwind scheme for ideal magnetohydrodynamics*, Journal of Computational Physics, 154 (1999), pp. 284–309.
  - [50] W. H. REED AND T. R. HILL, *Triangular mesh methods for the neutron transport equation*, tech. report, Los Alamos Scientific Lab., N. Mex.(USA), 1973.
  - [51] J. A. ROSSMANITH, *An unstaggered, high-resolution constrained transport method for magnetohydrodynamic flows*, SIAM Journal on Scientific Computing, 28 (2006), pp. 1766–1797.
  - [52] K. SCHNEIDER, S. NEFFAA, AND W. J. BOS, *A pseudo-spectral method with volume penalisation for magnetohydrodynamic turbulence in confined domains*, Computer Physics Communications, 182 (2011), pp. 2–7.
  - [53] C.-W. SHU, *Essentially non-oscillatory and weighted essentially non-oscillatory schemes*, Acta

- Numerica, 29 (2020), pp. 701–762.
- [54] E. TADMOR, *The numerical viscosity of entropy stable schemes for systems of conservation laws. I*, Mathematics of Computation, 49 (1987), pp. 91–103.
- [55] E. TADMOR, *Entropy stability theory for difference approximations of nonlinear conservation laws and related time-dependent problems*, Acta Numerica, 12 (2003), pp. 451–512.
- [56] G. TÓTH, *The  $\nabla \cdot \mathbf{B} = 0$  constraint in shock-capturing magnetohydrodynamics codes*, Journal of Computational Physics, 161 (2000), pp. 605–652.
- [57] L. WEI, L. ZHOU, AND Y. XIA, *The jump filter in the discontinuous Galerkin method for hyperbolic conservation laws*, Journal of Computational Physics, (2024), p. 113498.
- [58] K. WU AND C.-W. SHU, *A provably positive discontinuous Galerkin method for multidimensional ideal magnetohydrodynamics*, SIAM Journal on Scientific Computing, 40 (2018), pp. B1302–B1329.
- [59] Y. YU, Y. JIANG, AND M. ZHANG, *Free-stream preserving finite difference schemes for ideal magnetohydrodynamics on curvilinear meshes*, Journal of Scientific Computing, 82 (2020), pp. 1–26.